Dynamics of Entangled H-Polymers: Theory, Rheology, and Neutron-Scattering

T. C. B. McLeish,*,† J. Allgaier,‡,§ D. K. Bick,† G. Bishko,† P. Biswas,† R. Blackwell,† B. Blottière,† N. Clarke,† B. Gibbs,† D. J. Groves,† A. Hakiki,‡ R. K. Heenan,|| J. M. Johnson,⊥ R. Kant,† D. J. Read,† and R. N. Young‡

IRC in Polymer Science and Technology, Department of Physics and Astronomy, University of Leeds, Leeds, LS2 9JT, U.K.; Department of Chemistry, University of Sheffield, Sheffield, S2 2UN, U.K.; Institut für Festkörperforschung, FZ Jülich GmbH, 52425, Jülich, Germany; ISIS, Rutherford-Appleton Laboratory, Chilton, Oxon, OX11 0QX U.K.; and Department of Physics, University of Sheffield, Sheffield, S2 2UN, U.K.

Received March 3, 1999; Revised Manuscript Received June 24, 1999

ABSTRACT: We present experiments and theory on the melt dynamics of monodisperse entangled polymers of H-shaped architecture. Frequency-dependent rheological data on a series of polyisoprene H-polymers are in good agreement with a tube model theory that combines path-length fluctuation (like that of star polymer melts) at high frequency, with reptation of the self-entangled "cross-bars" at low frequencies (like that of linear polymer melts). We account explicitly for mild polydispersity. Nonlinear step-strain and transient data in shear and extension confirm the presence of a relaxation time not seen in linear response, corresponding to the curvilinear stretch of the cross-bars. This time is very sensitive to strain due to the exponential dependence of the branch-point friction constants on the effective dangling path length. Strain-induced rearrangements of the branch points are confirmed by small-angle neutron scattering (SANS) on stretched and quenched partially deuterated samples. We develop an extension of melt-scattering theory to deal with the presence of deformed tube variables to interpret the SANS data.

1. Introduction

The remarkable rheological properties of entangled polymer melts and solutions have continued to fascinate the polymer science community since the key developments of synthetic routes to monodisperse model polymers[1] and powerful molecular theories for melt dynamics. The most successful of these are based on the tube model of entanglements.[2] Well-defined experimental molecular architectures of small polydispersity are important because they provide quantitative tests for molecular theories. For example, the tube model gives very different predictions for entangled dynamics in the two cases of linear[3,4] and star-shaped[5,6] chains. Modeling the topological restrictions on a given chain from its neighbors as a confining tube of diameter a (of a size specific to each chemistry) along the chain contour, linear chains renew their configurations chiefly by a curvilinear diffusion called reptation (see Figure 1a). This leads to the prediction of a near single-exponential form of the relaxation modulus $G(t)$ and a dependence of the relaxation time τ_{rep} on molecular weight of M^3. Star polymers, however, are forbidden this route and must rely on the successively more unlikely path-length fluctuations to renew configurations of chain segments nearer and nearer to their branch points (see Figure 1b). Now a very broad range of relaxation times is predicted, corresponding to the different distances of segments from the free ends. The longest relaxation time (of the segments nearest the branch points) have an exponential dependence on the arm molecular weight. Both of these features are borne out by experiments on anionically polymerized monodisperse star and linear melts of different chemistries.[7] Of particular note is the independence of the viscosity on the number of arms of a star polymer (unless this is very large).

Recently, the tube model theory for star polymers has been developed to a high degree of refinement.[8] This work accounts for rapid Rouse-mode loss of entanglements at early times and a progressive dilution of the entanglement network at longer time scales such that $G(\Phi) \approx \Phi^{\beta}$ with $\beta = {}^7/_3$ and Φ as the concentration of unrelaxed segments.[9,10] When such a "dynamic dilution" of currently relaxing material by faster segments is accounted for in the tube model, the resulting expression for $G(t)$ is in quantitative agreement with data on star polyisoprenes covering over 5 orders of magnitude in viscosity.[7] This is true despite the small number (two) of free parameters of the model (the plateau modulus G_0 and a monomeric friction constant or equivalently the Rouse time of an entanglement length τ_e). These are furthermore constrained to be consistent with literature values from linear polymers. A natural consequence of the theory is the universality of melt rheology of flexible polymers, providing all molecular weights are expressed in terms of the entanglement molecular weight M_e. Values of M_e specific to many different chemistries are now available.[11]

Very recently, the theoretical tools developed to deal quantitatively with the path-length fluctuation modes of star polymers have been applied as corrections to the theory for linear chains:[12] the observed form of the high-frequency relaxation spectra emerge, together with the $\eta \approx M^{3.4}$ "law". Applications to controlled-architecture blends of star-with-star[13] and star-with-linear[14] polymers have recently been highly successful. Among other insights, the application of the theory to the star−linear blend has produced a criterion for when the simple

† University of Leeds.
‡ Department of Physics, University of Sheffield.
§ Institut Für Festkörperforschung.
|| Rutherford-Appleton Laboratory.
⊥ Department of Physics, University of Sheffield.

10.1021/ma990323j CCC: $18.00
Published on Web 09/09/1999

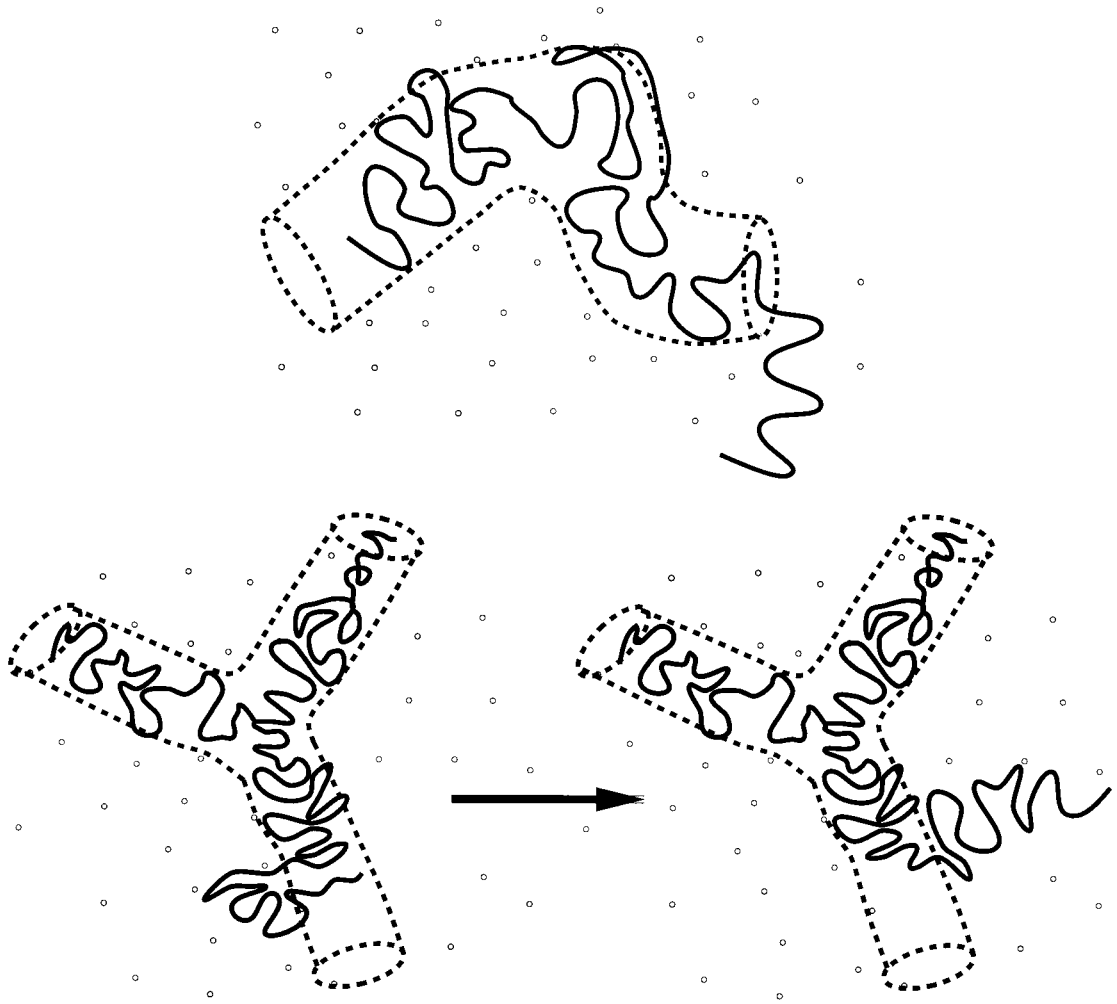

Figure 1. Diagrammatic representation of the processes of (a) reptation and (b) arm retraction via fluctuations for stress relaxation in linear and branched polymers, respectively.

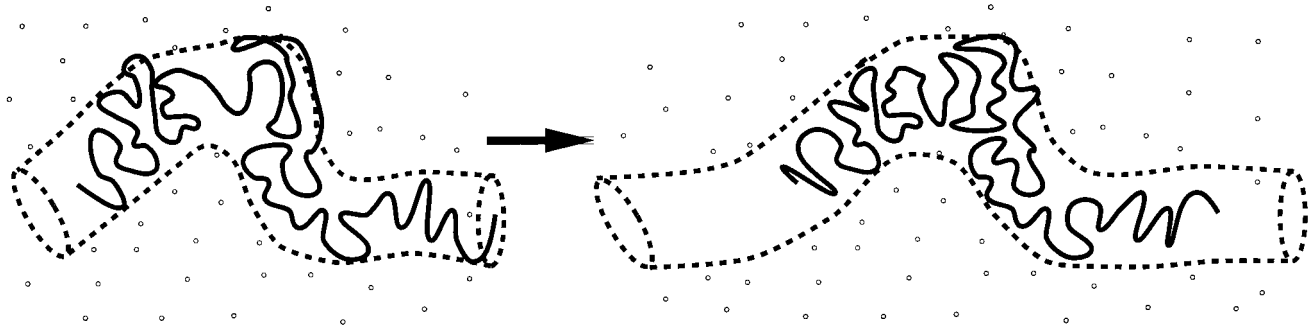

Figure 2. Retraction of chain in an extending tube in a nonlinear flow.

dynamic dilution treatment of constraint release[6] applies.

The time seems ripe to move on to a quantitative analysis of more complex architectures. The motivation for this also comes from the long-appreciated advantages of multiple long chain branching in commercial polymers such as low-density polyethylene (LDPE).[15] Although they are at least as shear-thinning as linear melts, in extension, these materials are strongly deformation hardening. Additionally, their "damping functions" (the factorable dependence on strain in a nonlinear shear step−strain experiment) are not as shear-thinning as those of linear polymers.[16] It might have been expected that such novel properties of branched polymers in nonlinear flows would be seen in monodisperse star polymers. However, they seem to be just as shear-thinning as linear melts, following a Doi−Edwards damping function,[7] at least in step shear. Within the framework of the tube model, this is not a surprise because the strong reduction of stress on large strains is explained by the rapid retraction of chains within strained (and so extended) tubes (see Figure 2). Such retraction is clearly not hindered in the case of star polymer melts because it depends on the high curvilinear mobility of the free ends. In star polymers, every piece of chain segment is topologically connected directly to a chain end, and so it may retract as rapidly within its tube as would a linear chain. This will not be the case for the next most complex topology of branched polymer, the H-architecture[17,18] (Figure 3). H-polymers

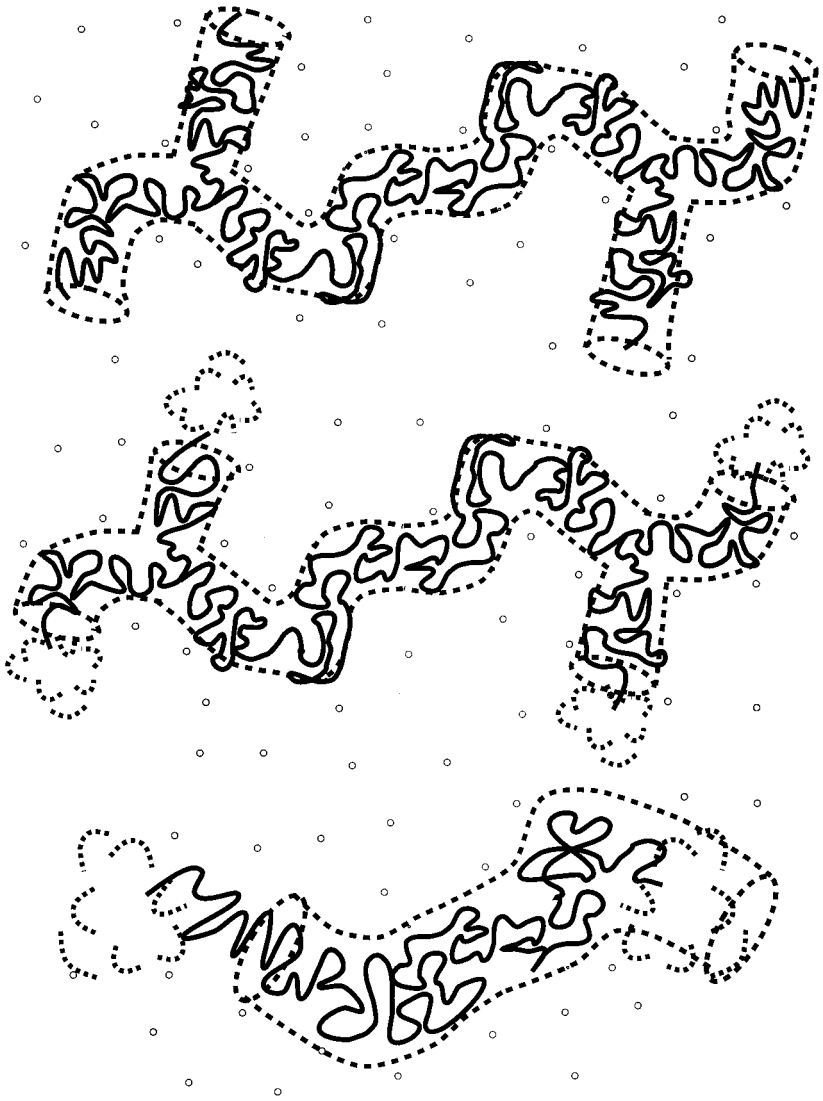

Figure 3. Three stages of stress relaxation in the H-polymer: (a) very early times at which only arm extremities have relaxed by Rouse breathing, (b) longer times at which significant fractions of the arms have relaxed by activated path-length fluctuation, and (c) relaxation of the cross-bar via renormalized reptation in a dilated tube. Frictional drag comes from the relatively rapid retractions of the dangling arms.

have four starlike arms, which must relax by path-length fluctuation in linear response, and are indeed free to retract rapidly after large strains. However, they are connected by a "cross-bar", a novel type of chain segment trapped between branch points. Under large strains, they are not free to retract rapidly (but see below for very high strains), thus suggesting qualitatively new dynamical behavior in this case. Yet at long time scales, when the dangling arms have completely relaxed, these slow central sections must behave as linear polymers (by dynamic dilution). So the H-polymer is expected to combine an intriguing combination of the features of star and linear polymers in linear response but exhibit a radical departure from both structures in nonlinear response. It shares this property with all comblike structures, of which it is the simplest member. A few studies both experimental[19] and theoretical[20] have been made on comb melts, but as yet, the synthesis of combs has always retained some stochastic element (in particular, in the position of side branches). For the present, the H-structure offers the best hope of a strictly controlled molecular architecture containing more than one branch point per molecule.

Recently, the tube model was applied to a generalization of the H-polymer possessing an arbitrary number of dangling arms on each branch point.[21] Predicted properties remarkably similar to those of LDPE in both shear and extension emerged. This work also made the remarkable prediction that a monodisperse "pom-pom" (or of course H-) melt will not possess a factorable step−strain response. Data on real polymer melts of such architecture is urgently required.

An early set of data on H-polystyrenes (PS)[17] was obtained on a series of molecular weights with equal amounts of material in each arm (M_a) and cross-bar (M_b). Three important observations were made: (i) the cross-bar did indeed provide relaxations at lower frequencies than those a melt of pure stars (of matching M_a) would have had; (ii) for most of these polymers, the low-frequency contribution appeared Rouse-like, having $G''(\omega) \approx \omega^{1/2}$ before the terminal time, with the highest molecular weights suggesting the emergence of a new low-frequency peak; (iii) plotting log η against the arm molecular weight M_a gave a straight line (i.e., exponential dependence similar to that of stars) but with a higher slope than that of star polymers. However, PS

has a large value of M_e of about 18 000; therefore, molecules of reasonably high molecular weight are still not highly entangled in the sense that $M_a/M_e \gg 1$ and $M_b/M_e \gg 1$. A subsequent initial theoretical approach to the H-polymer problem[18] predicted a much more marked peak in $G''(\omega)$ at low frequencies if the cross-bars were sufficiently well entangled to be forced to reptate at long times. This is a strong condition since the only entanglements available to the cross-bars at long times are those with other cross-bars (all arm material disengages from the entanglement network on much faster time scales than any motion of the cross-bars). The theory also conjectured that retraction would indeed be favored in strains larger than a critical strain to induce "branch-point withdrawal" (see below) when both cross-bar and arms were well-entangled. This new nonlinear mechanism has since been generalized to calculate the step−strain response of arbitrary topologies.[22] All of these predictions require a more heavily entangled polymer as a test material. These were the motivations behind the synthesis of a series of H-polyisoprenes (PI) that we have already reported.[23] PI has a much lower value of M_e of 3 800−5 000 depending on microstructure and a low glass-transition temperature (T_g). The first property allows H-polymer melts with a much greater degree of entanglement and a wider range of relaxation times to be synthesized using reasonable molecular weights; the second permits experimental access to the longest relaxation times that arise. In these circumstances, the rheological spectra do indeed show remarkable features at different time scales [in particular, in $G''(\omega)$] that seem to be identified with the relaxation of arms (fast) and cross-bar (slow).[25,26] This paper attempts to address these data quantitatively. Very recently similar features have been reported for a three-arm pom-pom polybutadiene architecture.[24]

Finally, we would like to exploit the structural predictions of the theories as well as those for bulk rheological response. Especially in the case of large strains, the tube model makes specific predictions about the configuration of individual chains following the retraction process. In the case of H-polymers, the additional feature of branch-point withdrawal has very specific consequences for molecular configuration that may be checked in principle by small-angle neutron scattering (SANS).[27] Flowing polymer melts with partial deuteration, quenched rapidly before exposing to a neutron beam, have shown how scattering becomes isotropic below a length scale related to the tube diameter.[28] However, quenched SANS experiments in extension of (weakly entangled) linear PS failed to give strong evidence of the tube retraction mechanism.[29] However, we might hope that the more strongly entangled PI would give clearer SANS signatures of the various retraction dynamics. In any case, the combination of such direct structural information with rheology is likely to provide a greater insight into any new physics that arises in these more complex architectures. The combination of SANS in tandem with rheology constitutes a powerful tool for examining molecular pictures of entangled polymer melt rheology. It involves special synthesis of partially labelled H-molecules and will require an extension of the current equilibrium theory for scattering from polymer melts, the "random phase approximation" (RPA).

In the next section, we derive the tube model theory for well-entangled H-polymers in linear and nonlinear step strain. In section 3, we describe the synthesis, rheology, and neutron scattering experiments. In section 4, we review the results in the light of the theory, including a discussion of the interpretation of the SANS patterns, then we conclude in section 5. Details of a number of calculations will be found in the appendices.

2. Tube Model Theory

As briefly discussed above, the goal of our theoretical development will be to make quantitative the insight that the existence of the tube constraint gives rise to a dynamical hierarchy of relaxation events in melts of entangled H-polymers. We consider both linear stress relaxation and nonlinear response after a step strain. Mathematical details are given in the appendices.

2.1. Linear Response. The implementation of the tube model for stress relaxation requires us to focus on the dynamics of the free ends of the polymer architecture in question, for it is generally true that stress is lost from a tube segment when a free end diffuses past it.[2] We take the dynamical processes that progressively liberate tube segments in the H-polymer in order of time scale. They are represented pictorially in Figure 3.

(i) At early times (following a small step strain), stress will relax by path-length fluctuation in the dangling arms. Just as for star polymers,[7] these fluctuations will be controlled at very early times by rapid Rouse motion of the chain end along the tube.

(ii) The rapid path-length fluctuation crosses over to an exponentially slow "activated diffusion" for the deeper arm fluctuations. The effective tube diameter grows continuously and self-consistently throughout this regime, and the cross-bars remain immobile.

(iii) After the starlike arms have completely retracted, the physical picture for the molecules changes to consider the mobility of the cross-bars in widened tubes defined only by their mutual entanglements. All of the effective friction is concentrated at the branch points. The rapidly fluctuating arms provide drag that far outweighs the sum of monomeric drags along the cross-bars. Initially, stress is lost from cross-bar segments via free independent diffusion of the branch points along the tube (analogous to the early curvilinear Rouse motion of the free arm ends).

(iv) The free curvilinear diffusion of the chain ends is suppressed when path-length fluctuations become slowed by the effective elastic potential (so thinking of the cross-bar as a "two-arm star" [14]). Central portions of the cross-bar are relaxed by reptation. This is the slowest contribution to the linear stress relaxation.

The strategy for turning this physics into a quantitative theory requires two steps:

(I) We must calculate a hierarchy of time scales $\tau(x)$ in terms of an arc coordinate or coordinates x that trace through the molecular segments from the extremities to the center. For example, in simple star polymer melts with monodisperse arms, x takes the value 0 at the chain ends and increases to 1 at the core where the arms meet. A more general arc coordinate x has elsewhere been termed the "seniority" in the context of an arbitrary branched polymer.[30]

(II) We then write a form for the effective modulus of an entanglement network diluted to a concentration $\Phi(x)$, where $G(\Phi) = G_0\Phi^\beta$ and $\Phi(x)$ is the concentration of unrelaxed material when segments with coordinate x are just relaxing (i.e., at the time scale when tube segments at x are just being reached by free ends for the first time). These are the assumptions of the

dynamic dilution hypothesis. Then, an expression for the relaxation modulus $G(t)$ may be written from the general expression

$$G(t) = \int_0^1 \frac{\partial G[\Phi(x)]}{\partial x} e^{-t/\tau(x)}\, dx \qquad (1)$$

(Without loss of generality, we may choose limits on x that are convenient). This expression assumes only that the effective modulus at time t depends on the amount of unrelaxed tube and is valid providing all currently unrelaxed chain has been able to explore fully the dilated tube at t. At time t, the unrelaxed fraction of chain is $\Phi[x(t)]$. If we assume the applicability of the dilution exponent β discussed in the Introduction, then the corresponding value of the tube diameter at t is just $a_{eff}(t) = a\{\Phi[x(t)]\}^{-\alpha/2}$ where $\alpha = \beta - 1$. This follows from the dependence $G \approx \Phi/M_e$ and the Gaussian form of chains in a polymer melt ($a \approx M_e^{1/2}$). The dynamic dilution assumption can break down for the very final stage of pure star relaxation and in star-linear blends,[14] but is safe in the context of H-polymer melts where the effective concentration Φ is a smooth function of the arc coordinate x right up to the branch point. In this case, the divergence of the effective tube diameter in the star polymer case is avoided by the contribution of cross-bar material to the entanglement network.

For H-polymers, it is natural to divide the arc coordinate into two sections: x_a runs along the arms from the ends to the branch points ($0 < x_a < 1$) and x_b runs from the branch point to the middle of the cross-bar ($0 < x_b < 1$). Now eq 1 becomes

$$G(t) = G_0(\alpha + 1)\left\{\begin{array}{l}\int_0^1 \phi_b^{\alpha+1}(1 - x_b)^{\alpha} e^{-t/\tau_b(x_b)}\, dx_b \\ + \int_0^1 (1 - \phi_a x_a)^{\alpha}\phi_a e^{-t/\tau_a(x_a)}\, dx_a\end{array}\right\} \qquad (2)$$

Here, ϕ_a and ϕ_b are the volume fractions of arms and cross-bar, respectively. The first term comes from the contribution of cross-bar material and the second from the relaxation of the dangling arms. In each integral, the term in round brackets represents the effective concentration of unrelaxed entangling network surrounding a segment relaxing on a time scale $\tau_{a/b}(x)$. We now turn to the derivation of the relaxation time scales for the dangling arms $\tau_a(x)$ and for the cross-bar $\tau_b(x)$. Here, we summarize as follows (for details, see Appendix A).

(i) The very outermost tube segments are relaxed by Rouse motion of the free end. This, like any monomer on a Rouse chain, has a spatial mean displacement s following the sub-Fickian form $s \approx t^{1/4}$, which, on inversion and substitution of the Rouse result in terms of monomeric friction, becomes[8]

$$\tau_e(x) = (225\pi^3/256)(N_a/N_e)^2\, \tau_R x^4 \qquad (3)$$

in terms of the Rouse time τ_R of the dangling arm.

(ii) Beyond an arc coordinate $x \approx (M_a/M_e)^{-1/2}$ fluctuations of the entangled path length of the arm begin to require unentangled folded loops either within the tube or emerging from its sides. These unusual configurations naturally cost in free energy amounts on the order of or larger than kT. The elastic free energy for such retractions in a fixed network was calculated by Pearson and Helfand[5] to be $U_0(x) = kT\nu s_a x^2$ with the constant $\nu = {}^{15}/_{8}$ and $s_a = (M_a/M_e)$. However, as we have seen, when activated retraction in such a potential occurs in entanglement environments composed of identical retracting material, the tube diameter relevant to further retractions at any time scale is diluted by all material occupying tube segments already relaxed. The only information needed in any specific case is the dilution of the entanglement molecular weight as a function of relaxed material fraction $M_e(x)$. The mathematical recipe for carrying out the consequent renormalization of the potential to the effective potential $U_{eff}(x)$ was given by Ball and McLeish[31] and is generally the solution of the differential equation

$$dU_{eff}/dx = \partial U_0[x; M_a, M_e(x)]/\partial x \qquad (4)$$

The application of this recipe to the activated retractions of H-polymer arms is discussed in Appendix A, where we give the form of the effective potential. It is easy to see, however, that the potential well is deeper and steeper than for pure star polymers, due to the fraction of cross-bar material that behaves as a permanent network for the relaxing arms. In this way, the fraction of arm material enters into the exponent for the longest relaxation time among arm retractions, which becomes

$$\tau_a \approx \exp\left[\frac{15 s_a}{4}\frac{1 - (1 - \phi_a)^{\beta}(1 + \beta\phi_a)}{\beta(1 + \beta)\,\phi_a^2}\right] \qquad (5)$$

The mean first-passage time for diffusers over such a potential barrier as $U_{eff}(x)$ can be calculated analytically for all x in terms of integrals over the potential (see Appendix A). By crossing over smoothly to eq 3 for small x, the spectrum of arm relaxation times $\tau_a(x)$ is calculated, including a weakly x -dependent prefactor. Even at this early level of our analysis, we notice one very important physical consequence of the cooperative nature of the arm relaxations: the longest relaxation time of the arms is exponentially dependent not only on the number of entanglements on each arm s_a but also on the arm fraction ϕ_a. Increasing the amount of material in the cross-bars, which acts as a permanent network throughout the relaxation of the free arms, greatly extends the slowest mode of the arms. So star-arms attached to cross-bars of an H-polymer melt would be expected to exhibit exponentially slower relaxation times than when they are attached to simple branch points as in a melt of pure stars. This is the reason for Roover's early observation[17] that the "viscosity enhancement" of dangling arms (over the value they would have as linear polymers) was much greater in his H-polystyrenes than in the corresponding stars. As a first result from eq 5, we predict that for H-polymers possessing equal molecular weights in each section, such as Roovers' polystyrenes[17] (so that $\phi_a = {}^4/_5$), the slope of the log η/s_a plot should be 1.46 times greater than that for star polymers. This is quite consistent with Roovers findings.

(iii) When the path length of the dangling arms eventually fluctuates to zero, corresponding to the free end retracing a path through the melt to the branch point itself, the branch point may make a diffusive hop through the melt. At this time scale of $\tau_a(1)$, the tube diameter is set only by other cross-bars so has a value $a^* = a\phi_b^{-\alpha/2}$. There is a slight uncertainty in the $O(1)$ number that relates the time scale of the hop to the mean hopping distance; therefore, we will set the effective curvilinear diffusion constant of the branch

point to the value

$$D_{\mathrm{b\ eff}} = \frac{p^2 a^{*2}}{2q\tau_{\mathrm{a}}(1)} \tag{6}$$

and let p vary universally but of order unity. In fact, we expect p to be rather smaller than that from the nature of the projection of spatial diffusion onto the curvilinear tube (see Appendix A). We will find (see Experimental Section below) that a value of $p^2 \simeq {}^1/_6$ will account well for the materials covered in this study. The parameter q is the number of dangling arms from each branch point. It is, of course, set to the value 2 throughout this work but may vary with more complex architectures in the future. A related uncertainty exists for the diffusion of star polymers within the tube model, although in that case the problem is actually harder because the very last stages of star-arm retraction are not effectively entangled and there is no definition of a^*. The diffusive motion of the ends of the cross-bar is initially responsible for the loss of orientation and stress from its outer segments. In an analogy with the free Rouse diffusion orientation loss from the dangling arms, we write the "early form" for stress loss from the cross-bars as $\tau_{\mathrm{be}} \approx x^2$ (for coefficient, see Appendix A). Note that the relaxation times depend on the cross-bar arc coordinate as x^2 rather than x^4 for the free ends. This is because the effective friction for motion of the branch points is concentrated at the branch points themselves − only a negligible correction comes from the true monomeric friction of the cross-bar chains themselves.

(iv) Just as for the dangling arms, the free-diffusive path length fluctuations are slowed for fluctuations that make a considerable change to the renormalized cross-bar path length. These will be penalized by an effective potential, which may be constructed by thinking of the cross-bars as two-arm stars for times less than their reptation time. A crossover formula for the spectrum of relaxation times $\tau_{\mathrm{b}}(x)$ is constructed in an analogous way (for details, see Appendix A). A final crossover to the reptation time of the cross-bars is also required, since their central sections will typically have starlike fluctuation times much longer than the center-of-mass reptation mode of stress-relaxation available to them (but not available to dangling ends of H's or star polymers). The reptation time is determined by the time taken for the cross-bar to diffuse the curvilinear length not already relaxed by fluctuation, and thus it is given by the self-consistent relation

$$\tau_{\mathrm{rep}} = \frac{75(1 - x_{\mathrm{c}})^2 s_{\mathrm{b}}^2 \phi_{\mathrm{b}}^{2\alpha} \tau_{\mathrm{a}}(1) q}{2\pi^2} \tag{7}$$

with $\tau_{\mathrm{b}}(x_{\mathrm{c}}) = \tau_{\mathrm{rep}}$. Such a procedure was implemented recently in a calculation of the relaxation spectra of ordinary entangled monodisperse linear polymers, intended to account quantitatively for the path-length fluctuation contribution to stress-relaxation.[12] Comparison with data covering a wide range of molecular weights was very favorable, and the theory gives a natural prediction of a dependence of viscosity on molecular weight of approximately $M^{3.4}$ for values of M/M_{e} up to 1000.

Figure 4 shows the frequency-dependent moduli calculated from the scheme outlined above in i−iv for a range of values of arm and cross-bar molecular weights (measured in entanglement units). The prominent

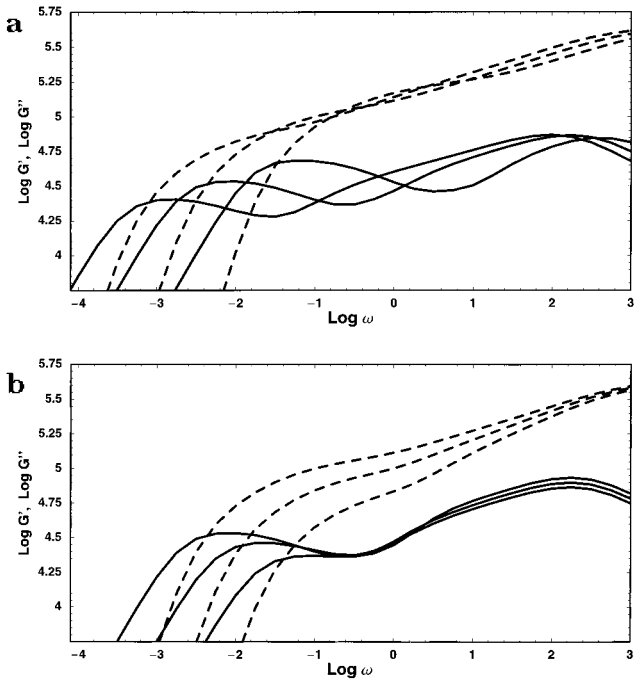

Figure 4. Predicted forms of $G'(\omega)$ and $G''(\omega)$ for a variety of H-polymer melts: (a) number of entanglements of the arms s_{a} of 4, 6, and 8 while the cross-bar s_{b} is fixed at 30 entanglement lengths and (b) s_{b} values of 20, 25, and 30 (in order of increasing terminal times) for fixed s_{a} of 6. Note the clear signatures of arm and cross-bar material and the much greater sensitivity of the spectrum to changes in the arm molecular weight.

"shoulder" feature at higher frequencies in $G''(\omega)$ is a clear signature of the arm relaxations; its logarithmic width increases with the arm molecular weight. The low-frequency peak comes from the cross-bar: lengthening the cross-bar takes the peak to lower frequencies, whereas reducing it both speeds up the cross-bar relaxation and weakens the magnitude of the peak as the volume fraction ϕ_{b} reduces and, with it, its contribution to the modulus (as $\phi_{\mathrm{b}}^{\beta}$). So the H-polymer spectrum we expect contains features reminiscent of the spectra of both star [a broad shoulder in $G''(\omega)$] and linear polymers [a well-defined peak in $G''(\omega)$] at the frequencies corresponding to the inverse relaxation time of the structural components that resemble them (arms and cross-bar, respectively).

An earlier calculation for the relaxation spectrum of the cross-bar contribution alone[18] differed from this scheme in two ways. First, an approximate value for the dilution exponent of $\beta = 2$ was taken; second, the fluctuation and reptation modes were more rigorously combined in a partial differential equation for relaxation by first passage of a free end in both center-of-mass and path-length spatial variables. This was solved numerically. The advantage of the present scheme is that it provides explicit analytical expressions for the whole spectrum of relaxation times throughout the molecule while embodying a highly accurate approximation to the 2-D coupled PDE.

2.2. Nonlinear Step Strain. The original success in accounting for the shear-thinning damping function of linear polymer melts was the first quantitative achievement that drew attention to the tube model,[2,16] and thus, it becomes an important investigation in the exploration of any more complex architecture. A stiffer response in step shear is measured experimentally in commercial

branched polymers (but not star polymers).[16] The inhibited retraction expected in branched polymers with more than one branch point has been used to calculate the stress immediately following a large step strain in the case of H-polymers[18] and tree, comb, and randomly branched architectures.[22] In this section, we review the calculation for H-polymers and extend it to the full time and strain dependence of the stress after a step shear $G(t, \gamma)$. For details, see Appendix B.

The initial deformation may described by the tensor **E** defined so that an arbitrary vector **v** in the material is deformed affinely into the vector **E**·**v**. For example, in simple shear of shear strain γ, and in uniaxial extension of strain ϵ, the tensor **E** takes the following forms:

$$\begin{pmatrix} 1 & \gamma & 0 \\ 0 & 1 & 0 \\ 0 & 0 & 1 \end{pmatrix} \quad \text{and} \quad \begin{pmatrix} \epsilon & 0 & 0 \\ 0 & \epsilon^{-1/2} & 0 \\ 0 & 0 & \epsilon^{-1/2} \end{pmatrix}$$

A general formula that may be used to calculate the stress within the tube model reads as follows:

$$\boldsymbol{\sigma} = kT\,(f/f_{eq})\,\langle c_a(\mathbf{u})\mathbf{u}\mathbf{u}\rangle \tag{8}$$

Here, (f/f_{eq}) is the ratio of the Brownian tension[2] along entangled chains to its equilibrium value, and $c_a(\mathbf{u})$ is the concentration of entanglement segments in the direction specified by the unit vector **u**. The orientational part of the stress tensor is given as usual by the average over the outer products of segment orientations **u**. Under a strain, the proportion of such entanglement strands is increased by a factor $|\mathbf{E}\cdot\mathbf{u}|$. This needs to be inserted inside the average over all initial orientations **u**. The unit vector itself changes naturally only in direction to $\mathbf{E}\cdot\mathbf{u}/|\mathbf{E}\cdot\mathbf{u}|$. The other modification is to the overall concentration of entanglement strands c_a. The retraction process means that the same proportion of original entanglement strands is lost as the length retracted; therefore, c_a is reduced along each chain by the factor $\langle|\mathbf{E}\cdot\mathbf{u}|\rangle$. Note that we may preaverage in the limit of many entanglement lengths per chain because a well-entangled chain explores all orientations in its tube segments.

The final result for the stress-tensor in the case of linear polymer melts is that

$$\boldsymbol{\sigma} = kTc_{eq}\mathbf{Q}(\mathbf{E}) \tag{9}$$

where the geometric tensor **Q** is defined by the orientational averages over the unit vector **u**:

$$\mathbf{Q} = \frac{1}{\langle|\mathbf{E}\cdot\mathbf{u}|\rangle}\left\langle\frac{\mathbf{E}\cdot\mathbf{u}\;\mathbf{E}\cdot\mathbf{u}}{|\mathbf{E}\cdot\mathbf{u}|}\right\rangle \tag{10}$$

The averages may be written in spherical polar coordinates as angular integrals, which are simple to evaluate numerically, and in some cases have analytic forms.[2]

In the case of H-polymers, we need to make two modifications.[18] First, we recognize that immediately following a step strain only the dangling arms are free to retract along their contours. Second, an important consequence of the tube model is that a new type of retraction is nevertheless permitted at very high strains. Termed branch-point withdrawal;[22] it permits, in the case of H-polymers, the cross-bar to drag arm material into its tube when it becomes sufficiently stretched (see Figure 5). The criterion for onset of branch-point withdrawal is simply an entropy maximization in the connected rubber-elastic strands of the molecules. When the loss of entropy due to further stretching of the cross-bar would be greater than that due to double-occupation of tube segments by both dangling arms, the arms will no longer support further extension of the cross-bar. An alternative and equally valid criterion is to evaluate the balance of Brownian tensions in the various segments of the molecule. When the cross-bar tension is exactly twice the tension in the dangling arms, further extension will lead to branch-point withdrawal (we assume that the dangling arms possess the equilibrium tension since that is the value recovered after rapid retraction in the absence of strain-induced deformations of the tube diameter itself[6]). For segments that do not retract, there is no loss of entanglement density, but the curvilinear tension increases above its equilibrium value proportionally to the orientationally averaged extension of the tube length via the strain-dependent function $\alpha(\mathbf{E}) \equiv \langle|\mathbf{E}\cdot\mathbf{u}|\rangle$. Enumerating the stress contributions from arms and cross-bar of the H-polymer leads to an expression for the stress immediately following all rapid retractions (on the time scale of the Rouse time of the segments) of

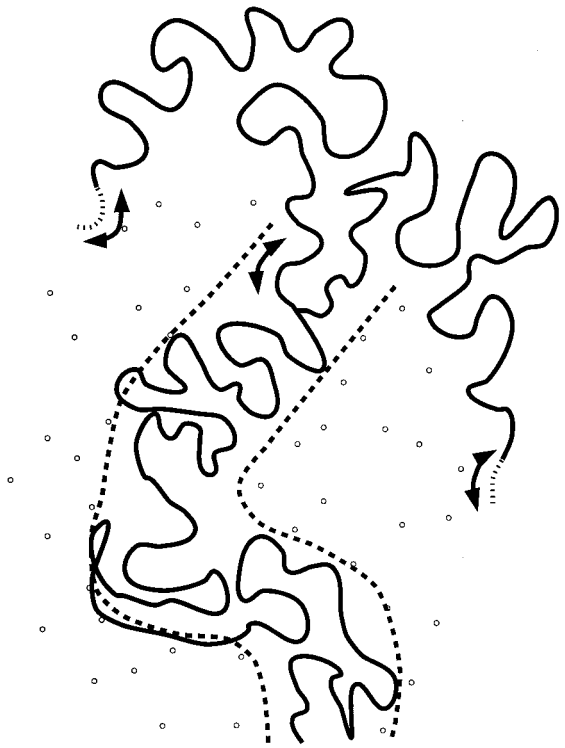

Figure 5. Partial withdrawal of a branch point into the tube previously occupied by cross-bar material. Mobility within a single tube volume may be rather high. Withdrawal causes deutero-labeled ends of the dangling arms to approach each other.

$$\boldsymbol{\sigma} = \begin{cases} \phi_b[\alpha(\mathbf{E})]^2\,\mathbf{Q}(E) + \phi_a\mathbf{Q}(E) & \alpha(\mathbf{E}) < 2 \\ \phi_b 4\mathbf{Q}(E) + \phi_a\mathbf{Q}(E) & \alpha(\mathbf{E}) > 2 \end{cases} \tag{11}$$

The next step is to extend this expression to an explicit theory for the stress relaxation following a large step strain $G(t, \gamma)$. There are some clear boundaries set by the physics we have already invoked. Perhaps initially the most surprising is that, at the terminal (reptation) time of the H-polymer melt, the damping

function derived from such an experiment should be the original universal Doi−Edwards form (derived from eq 10). This follows from the renormalized picture of the molecules at long times as mutually entangled (linear) cross-bars with dangling arms not contributing to the entanglement network. The question of how the response governed by eq 11 (and its generalizations to "early-time damping functions" for more complex architectures[22] at times of order $\tau_e s_a^2$ relaxes into the Doi−Edwards form of eq 10 at times of order τ_{rep} is answered by identifying a new dynamical mode unrepresented in linear response. This is the stretch relaxation of the cross-bar. The dynamics are generated by the entropic elasticity acting to restore its equilibrium path length working against the effective friction constant of the branch points $\zeta_{eff} = kT/D_{eff}$. This stretch mode is very important in the predicted constitutive behavior of the more general pom-pom polymer melt.[21] If we denote the ratio of the path length of the backbone to its equilibrium length as $\lambda(t)$, then we may generalize the evaluation of occupied entanglement segments and cross-bar chain tension that led to eq 11 to arbitrary times following the step strain to give

$$\frac{G(t)}{G_0} = \frac{Q_{xy}}{\gamma}(\alpha + 1) \times \begin{Bmatrix} [\lambda(t)]^2 \int_0^1 \phi_b^{\alpha+1} (1 - x_b)^{\alpha} \, e^{-t/\tau_b(x_b)} \, dx_b \\ + \int_0^1 (1 - \phi_a x_a)^{\alpha} \, \phi_a e^{-t/\tau_a(x_a)} \, dx_a \end{Bmatrix} \quad (12)$$

In the case of all deformations up to the critical strain for branch-point withdrawal, the initial value of $\lambda(0)$ is just $\alpha(\mathbf{E})$. The essential physical assumptions behind the combination of the linear stress relaxation from of eq 2 and the nonlinear step strain of eq 11 is that constraint-release from relatively rapidly relaxing extremities of the cross-bar does not affect the stretch relaxation of the principle mode describing the path length between the branch points. The relative stretch of the cross-bar contributes quadratically to the stress because a larger stretch will occupy proportionally more tube segments than a fully retracted chain, and at a proportionally higher effective tension.[21]

The problem is now reduced to the calculation of the time-dependent stretch. A simple model, which leads to single-exponential decay, was presented in the derivation of the pom-pom constitutive model.[21] By balancing the elastic and drag forces on the branch points at times longer than $\tau_a(1)$, the result is

$$\lambda(t) = 1 + [\lambda(0) - 1] \, e^{-t/\tau_s} \quad (13)$$

where the stretch relaxation time τ_s is given by

$$\tau_s = 5 s_b \phi_b^{\alpha} \tau_a(1) \quad (14)$$

For details, see Appendix B. Note that this is a new time scale not appearing in the linear relaxation spectrum. Its proportionality to the first power of the number of entanglements in the (renormalized) backbone means that it is generally intermediate to the longest relaxation time of the arms $\tau_a(1)$, and the reptation time of the cross-bar, $\sim\tau_a(1)s_b^2$. The prediction of this new time scale for nonlinear relaxation with a value typically 1 order of magnitude or less than the terminal time was shown to be of fundamental importance in producing the special extension hardening and shear overshoot behavior of the pom-pom class of polymer melts, of which the H-polymer is the simplest example.[21]

Such a simple approach gives a very qualitative idea of the essential dynamics but, as we shall see, does not do justice to the data in step strain (see section 3). The experiments indicate that the stretch relaxation process does indeed appear but that its relaxation time scale is highly dependent on the initial imposed strain. A more thoughtful approach to the model shows why this might be expected. We have seen that the branch point is not withdrawn into the cross-bar tube at strains lower than the critical (bulk) strain of about 400%, when it achieves the maximum permitted tension of $2f_{eq}$. However, the increased tension in the cross-bar will certainly induce an increasing displacement of the branch point away from the dangling arms' tubes of up to a tube diameter a at rather smaller strains (see Figure 5). At first sight, this would not seem to perturb the dynamics significantly, until we recall that all dynamical modes of the cross-bar depend on the magnitude of the effective diffusion constant of the branch points and that this in turn is exponentially dependent on the entangled path length of the arms. Reducing this path length by even one section of length M_e changes the retraction time significantly. The factor is not universal because the effective potential for arm retraction depends on the overall fraction of arm material ϕ_a from eq 5. We may write in general $\tau_a(1) \approx \exp(\nu' s_a)$, where ν' is 15/8 in the limit of low arm fraction and 27/56 in the limit of high arm fraction (a pure star melt). Moreover, the actual path-length withdrawn depends on the strength of the effective localizing potential which works to keep the branch point central in the surrounding tube-network. The relevance of this potential is another new feature of multiply branched polymer melts. Its effective localization length is clearly on the order of the current effective tube diameter but may conceivably vary by an $O(1)$ prefactor. Toward the limit of low arm-fraction, such a local rearrangement of material in tubes around branch points may reduce the effective friction constant of the branch point by a factor of around 7, without the onset of the more drastic branch-point withdrawal.

The simplest way to build this physics into a model for cross-bar stretch relaxation is to suppose that the tube around the branch points serves to localize them with a quadratic potential field,[32] which we write as

$$U_{loc}(s) = q\frac{kTs^2}{(wa)^2} \quad (15)$$

The extent of the potential must be such that the quadratic displacement matches the gradient of the effectively linear (constant force) potential for displacements of the branch point of greater than one M_e (branch point withdrawal). The displacement of the branch-point for any given stretch λ of the cross-bar is then allowed to modify the effective friction of the branch points via the exponential form $\tau_a(1) \approx \exp(\nu' s_a)$. The nonlinear differential equation for $\lambda(t)$ that results is

$$\frac{\partial\lambda(t)}{\partial t} = -\frac{(\lambda(t) - 1)}{\tau_s} \exp[\nu^*(\lambda(t) - 1)] \quad (16)$$

where the exponential nonlinearity is clearly modifying an otherwise simple exponential relaxation to the equilibrium value of $\lambda = 1$. We might expect to find that the

constant ν^* is of order unity, but it grows with the dimensionless range w of the effective localizing potential U_{loc}. The derivation of and various approximation schemes for the solution of eq 16 are discussed in Appendix B. The central result is that the initial relaxation rate of stretch following a large strain can be much larger than τ_s^{-1}. The long time decay will fall back onto this characteristic time scale but with a lower relative amplitude than that in linear response. Such behavior will naturally induce similarly fast decay in $G(t, \gamma)$ via eq 12.

The special molecular configurations invoked by this theory of nonlinear strain also motivate the neutron scattering experiment described in the next section. Before going on the discuss the experiments, however, we draw on our lesson about the high sensitivity of the branch-point diffusion constants and anticipate some aspects of the role of polydispersity.

2.3. Polydispersity. Even though the materials investigated here were anionically polymerized, achieving the highest possible standards of monodispersity, we might expect the exponential sensitivity of the branch-point diffusion constant of the path length of the arms to amplify any slight polydispersity, especially in the molecular weights of the arms. Calculations on arbitrary distributions via a moment analysis (see Appendix C) show that polydispersity induces two effects on the relaxation spectrum at times longer than $\tau_a(1)$: (i) a positive shift of the mean relaxation time, and (ii) a spread of the relaxation times. In the H-polymer spectra, these may be particularly evident in the position and shape of the "reptation peak" at low frequencies. Writing $M_w/M_n = 1 + \epsilon$, we find that small polydispersity effectively renormalizes the number of entanglements along an arm s_a to

$$s_{ar} \approx s_a + \frac{\nu' s_a^2}{2}\epsilon_a \qquad (17)$$

So in the case of a good anionic polymerization in which $\epsilon = 0.05$, a polymer with a moderate ϕ_b such that $\nu' = 1$ and with arms of six entanglement segments, the terminal time undergoes a relative shift of $\simeq 3$ and a relative spread of as much as $^1/_3$. The spread in particular increases rapidly with the molecular weight of the dangling arms, however well-controlled the polydispersity. A similar effect arises in the contributions to the relaxation spectrum arising from the cross-bar because in practice a significant fraction of cross-bar material relaxes by fluctuation modes (see Appendix C). Such a strong effect of polydispersity might have been expected in the simpler case of star polymers. However, in that case, the mutual retraction dynamics proves to be strongly motion-narrowing.[31] It is the presence of slowly relaxing cross-bar material that "amplifies" the inherent polydispersity of the arms' relaxation times.

2.4. Transient Response. It is possible to use the tube model we have developed to predict the response of an H-polymer melt in transient viscometric flows without introducing any more physical assumptions. In particular, if deformation rates are considered up to those on order of the inverse stretch time τ_s^{-1}, then the faster-relaxing arm material will be in linear response. All nonlinear behavior will arise from the cross-bar segments. Equation 12 may in this case be generalized to a constitutive equation for arbitrary flows using the approach of the pom-pom constitutive derivation.[21] The active (slow) segments of the cross-bar possess an orientation distribution $\mathbf{S}(t, x_b)$ for tube segments at coordinate x_b. These relax by the fluctuation-modified cross-bar reptation process at τ_{rep} for $x_b > x_c$ and by the fluctuation timescales $\tau_b(x_b)$ for $x_b < x_c$. They will couple to the flow just like a segment of Doi−Edwards linear polymer via an integral over past times. In addition, they also possess the important stretch variable $\lambda(t)$ that relaxes with the (current) value of τ_s but is also driven in a flow by the instantaneous rate of tube stretching. Unlike the orientation $\mathbf{S}$, the stretch λ is uniform along the cross-bar for all deformation rates that interest us because local stretch is rapidly distributed along the chain via its fast Rouse modes. The growth and decay of λ is also uniform along the cross-bar because these couple to the flow via the average along the cross-bar chain of the orientation average $\langle \mathbf{S}(t), x_b \rangle_{x_b}$, and via the current effective values of the branch-point drag coefficients. So in an arbitrary flow history of local deformation gradient $\mathbf{K}(t)$, the constitutive equation becomes

$$\sigma(t) = G_0 \{ {}^{15}/_4 \phi_b^{\alpha+1}(1 - x_c)^{\alpha+1} [\lambda(t)]^2 \mathbf{S}(t, 1) + {}^{15}/_4(\alpha + 1)[\lambda(t)]^2 [\int_0^{x_c} \phi_b^{\alpha+1}(1 - x_b)^\alpha \mathbf{S}(t, x_b)\, dx_b + \int_0^1 (1 - \phi_a x_a)^\alpha \phi_a \int_{-\infty}^t (\mathbf{K}(t') + \mathbf{K}^T(t'))\, e^{-(t-t')/\tau_a(x_a)}\, dt'\, dx_a] \} \qquad (18)$$

with the orientation tensor given by the history integral:

$$\mathbf{S}(t, x_b) = \int_{-\infty}^t \mathbf{Q}[\mathbf{E}(t, t')] e^{-(t-t')/\tau_b(x_b)}\, dt' \qquad (19)$$

and the cross-bar stretch factor by the coupled differential equation:

$$\frac{\partial \lambda(t)}{\partial t} = (\mathbf{K}:\langle \mathbf{S}(t, x_b) \rangle_{x_b})\, \lambda(t) - \frac{(\lambda(t) - 1)}{\tau_s} \times \exp[\nu^*(\lambda(t) - 1)] \qquad (20)$$

with the stipulation that $\lambda(t)$ remains less than or equal to the maximum cross-bar stretch of q set by branch-point withdrawal. The first term of eq 18 records the stress contribution from the central sections of the cross-bar that relax at the reptation time; the second term takes account of those cross-bar segments relaxing faster than τ_{rep} (though which also may be stretched in the flow). The third term arises from arm material, which is taken to be in linear response at the flow rates we will consider ($|\mathbf{K}|\tau_a(1) \ll 1$). At this point, we have no detailed microscopic theory for the exact range of the localization potential for the branch point in its corresponding nexus of tubes. However, we might expect the range to be of order a, in which case ν^* would be of order 1. In practice, we only compute with eq 18 in transient flows for startup of simple shear and uniaxial extensional flows to address experimental data on the model H-polymers of this study.

3. Experimental Section

We report experimental rheology and SANS on four H-shaped polyisoprenes. Three were purely hydrogenous, and one was partially deuterated at the tips of the dangling arms. The linear rheology on all four polymers over a wide range of time scales was designed as a test of the theory for the spectra of molecular relaxation times outlined in section 2 above. The nonlinear−step strain rheology and neutron-scattering experiments combined to explore the more speculative extensions of the model to large strains.

Table 1. Molecular weights of Arms, Cross-bars, and Whole Molecules

polymer	arm SEC[1]/MO[2]	cross-bar SEC[1]/MO[2]	H-pol (M_n) predicted	H-pol (M_n) SEC[1]/MO[2]	H-pol (M_w) LALS
H110B20A	20 000[2]	111 000[2]	191 000	198 000[2]	219 000
H160B40A	40 000[1]	164 000[1]	324 000	324 000[1]	345 000
H200B65A	63 000[1]	198 000[1]	450 000	460 000[1]	612 000
H110B52A[a]	52 500[2]	111 000[2]	321 000	310 000[2]	334 000

[a] Contained a deuterated block of $M_n = 10\,000$ at the end of each arm (calculated from SEC using h-PI as a calibrant).

3.1. Synthesis. We give here an outline of the synthetic route. All manipulations were performed under high vacuum in glass reactors, provided with break seals for the addition of reagents. The arms of the H-polymers were synthesized as monofunctional polyisoprenyllithium chains in one reactor using *s*-BuLi as an initiator and benzene as solvent. In the case of the partially deuterated H-polymer arms, a second quantity of hydrogenous isoprene was added after polymerization of the deuterated monomer was complete. The cross-bars were synthesized in another reactor using the 2:1 adduct of *sec*-butyllithium and 1,2-bis[4-(1-phenylethenyl)phenyl]ethane as a difunctional initiator. Lithium *sec*-butoxide was needed as a promoter for the difunctional initiator. In both cases, the reaction was run to completion in 48 h. In a second step, a large excess of MeSiCl3 (~50:1) was added to the difunctional chains for a further 24 h, after which excess trichlorosilane was removed under vacuum together with solvent. In the final stage, the monofunctional chains were added in excess to the telechelic together with the promoter triethylamine and the reaction was allowed to continue for 3 weeks. The reaction was terminated by quenching the excess of living chains with methanol, and the polymer fractionated as a 1% solution in toluene as solvent and methanol as precipitant. The microstructure of the polymers was determined by ^{1}H NMR spectroscopy. For the arms as well as the cross-bars, it was found that the polymers contain 93−95% of 1,4-units and 5−7% of 3,4-units. Molecular weights of arms, cross-bars, and whole molecules were measured by size exclusion chromatography (SEC), membrane osmometry (MO), and light scattering (LALS). Results on the four polymers used in this work are tabulated in Table 1.

3.2. Rheology. Linear rheological spectra were obtained in oscillatory shear between parallel plates. Data from two machines, a Rheometrics RDA II and RDS, were combined. Temperatures from −30 to 150 °C were used to cover an effective frequency range of 10^{-6}−10^5 rads^{-1} at 25 °C by time−temperature superposition. All strains were measured to be in the range of linear response. In all cases except the very large H200B65A, the terminal zone was reached. Repeated measurements after runs at the highest temperatures did not detect any significant degradation. Carrying out the rheology under a nitrogen atmosphere and in the presence of added antioxidant helped to ensure sample stability.

Nonlinear step stain experiments were carried out on the same instruments but in cone/plate geometry. Considerable care was needed in loading and compressing the samples. Initial strains of 1, 10, 30, 100, 200, 250, and 500% were imposed within 0.1 s, and the time-dependent stress calculated from the decay of measure torque. Consistency of the data was checked by using a range of cone angles from 1 to 5°. Significant departures from consistency toward greater apparent strain-softening were evident beyond strains of 100% at the larger cone angles; this effect could be delayed to beyond 1000% for the smallest cone angles. The problem is consistent with an edge instability characteristic of cone/plate deformations of highly elastic liquids.[33] Data presented here was taken from cones with 1 and 1.5° angles, below the strain at which we identified the instability to set in.

The transient growth of the shear viscosity was measured with a cone and plate geometry using a Rheometrics RDA II rotational rheometer. A cone and plate diameter of 10 mm with a cone-to-plate angle of 1° was used, partly due to the very small laboratory-scale quantity of polymer available. A 10 mm diameter disk specimen, cut from the prepressed sheet, was squeezed progressively between the truncated cone and plate at 90 °C in a nitrogen atmosphere, allowing the normal forces to relax, until the polymer conformed to the correct geometry. The small-diameter cone and plate allow large normal stresses within the normal force limit of the transducer while initially squeezing the specimen. The small cone-to-plate angle minimizes the risk of edge fracture.[33]

Measurements were made at shear rates from 0.003 to 3 s^{-1} using the rheometer in steady shear mode. The polymer was taken to various total shear strains, typically 15 at 0.003 s^{-1} to 150 at 3 s^{-1}, to demonstrate either a viscosity plateau or overshoot.

All of the polymer specimens were cross checked by their dynamic $G(\omega)$ "fingerprint" using the same rotational rheometer.

The transient growth of the extensional viscosity was measured on thin slabs of material in a modified Rheometrics RME extensional rheometer. This device provides a constant extension rate to a sample by gripping it between counter-rotating caterpillar tracks. The sample is both heated and suspended mechanically over a rising current of temperature-controlled nitrogen. Due to the small amounts of model polymer available, rather smaller samples than usual were employed. Preparation was by pressure-annealing finely divided pieces of the rubbery polymer in a press, giving sample dimensions of 0.5 × 4 × 60 mm^3. Choice of experimental temperature proved very important for sample stability; all data reported were obtained at 90 °C. Extension rates were varied between 0.003 and 1 s^{-1}, and uniformity of the sample checked by direct video imaging.

3.3. Small-Angle Neutron Scattering. To test the predictions of partial branch-point withdrawal on large strains, the partially deuterated polymer was solvent-cast into sheet approximately 0.5 mm thick from which samples measuring approximately 10 × 30 mm^2 were cut. All solvent was extracted by leaving the samples at room temperature under vacuum for 1 week. These were subjected to a rapid extensional strain in for ~0.1 s in a simple sliding double-clamp device and then quenched to below their glass-transition temperature in liquid nitrogen to freeze all further relaxation while the relatively long exposure to the neutron beam was made.

The strain rig was made from brass blocks and rod on which one block was free to slide. The sample was held in spring-loaded grips between this block and a stationary one. A 9.5 mm diameter cadmium aperture held onto the device defined the beam position. Stops could be inserted to determine the final strain of the sample after the sliding block reached its maximum traverse. To minimize the time taken by the strain, the sliding block triggered a holding catch on hitting the end stop. This permitted the whole assembly to be plunged into liquid nitrogen within 0.1 s of the imposed strain. From the linear rheology measurements, about 0.5 of the arm primitive path would have been reoriented by this time, as well as the rapid retraction, but all motions of the backbone and inner parts of the arm would have effectively been quenched.

After it was ensured that the whole assembly had reached T_g for PI, the assembly was transferred rapidly to a helium cryostat containing thin aluminum windows and heat shields through which the neutron beam passed largely unscattered. The brief transfer period (<1 s) permitted a visual inspection of the sample to ensure its integrity before embarking on the scattering experiment. The cryostat was evacuated to a very low helium pressure and held at −130 °C throughout the experiment. Small-angle scattering measurements were carried out on the LOQ instrument at the ISIS pulsed spallation source, Rutherford-Appleton Laboratory, Didcot, U.K. Time-of-flight enables simultaneous use of neutrons of wavelengths $\lambda = 2.2$−10 Å to obtain a wide range of scattering vector $|\mathbf{q}| = 2\pi \sin(\theta/2)/\lambda$ from 0.008 to 0.25 Å^{-1} using a 65 cm square detector at 4.05 m from the sample. Data normalization allows for the wavelength dependence of the incident spectrum, the detector response and the sample transmission.[34] In our case, the normalization could not accurately be quantitative because of uncertainties in the thickness of the highly rubbery samples

and the extent to which they filled the beam at large stretches. Background scattering from the empty sample holder within the cryostat was subtracted, and the SANS cross section was rescaled to absolute thickness using estimates of the thickness and width of the sample at each strain. Some nominally flat "incoherent" (elastic and multiple inelastic scattering) signal remains, due to the hydrogen atoms in the sample; thus, adjustable flat backgrounds were included in the fits described below. Exposure times ranged from 1 to 6 h to obtain reasonable statistics for anisotropic scattering from the increasingly thin samples.

4. Results and Discussion

4.1. Linear Rheology. Linear rheological spectra are given in Figure 6 for the four H-polymers in this study together with the results of the theory developed in section 1 for each case. The first remarkable feature that strikes the eye straight away is the obvious rheological "signature" we expect from the entangled H-shaped structure. This is particularly clear in the shape of the $G''(\omega)$ curves. Free Rouse modes within the tube at high frequencies give $G''(\omega) \approx \omega^{1/2}$. Progressing to lower frequencies, there is a minimum at $\omega \approx t_e^{-1}$, when entangled modes set in. This is followed by an extended shoulder feature whose width grows approximately linearly (on a log ω plot) with the length of the dangling arms. Finally, there is a weak maximum or step at lower frequencies coming from the relaxation of the cross-bars. The more highly entangled the cross-bars are with themselves, the more sharply defined is their reptation peak. So, the clearest signal comes from the sample H110B20A. This combines the advantages of a relatively high cross-bar fraction ϕ_b (so that the reptation peak has a reasonable magnitude) with a high degree of renormalized entanglement $s_b\phi_b \approx 15$ (so that the reptation peak is well-separated in time from the longest arm fluctuation time $\tau_a(1)$). The advantage of the low entanglement molecular weight of PI is already evident in the high degree of structure in the complex modulus.

The qualitative behavior is therefore as we expect. Quantitative consideration requires careful comparison with curves calculated for $G^*(\omega)$ from the theory of section 2. In each case, we show the predictions of the theory with and without the allowance for small polydispersity. This was treated at the relatively crude level of incorporating only the resulting shifts in the relaxation times. Especially for the lower molecular weight H-polymer, the difference is very marked indeed. As we saw in section 2, this is entirely consistent with the exponential dependence of the effective branch-point friction on the molecular weight of the dangling arms. In this way the polydispersity of the dangling arms is much more important than that of the cross-bars, even though the latter is rather larger, due to their difunctional polymerization route. Because of the slight uncertainties in molecular weight and polydispersities, the procedure adopted in each case was to vary the values of M_a and M_b and the polydispersities of arm and backbone via $\epsilon = M_w/M_n - 1$, until a fit with the data was obtained (itself not guaranteed!) and then to check consistency with the results of other standard characterization methods reported above. The two universal (for PI) parameters G_0 and τ_e were also allowed minor adjustment within the range represented by rheology on samples with different synthesis but remained within factors of 1.2 of 0.52 MPa and 7×10^{-6} s at 25 °C. This was the protocol adopted recently for a range of simple PI star polymers exhibiting a similarly wide range of

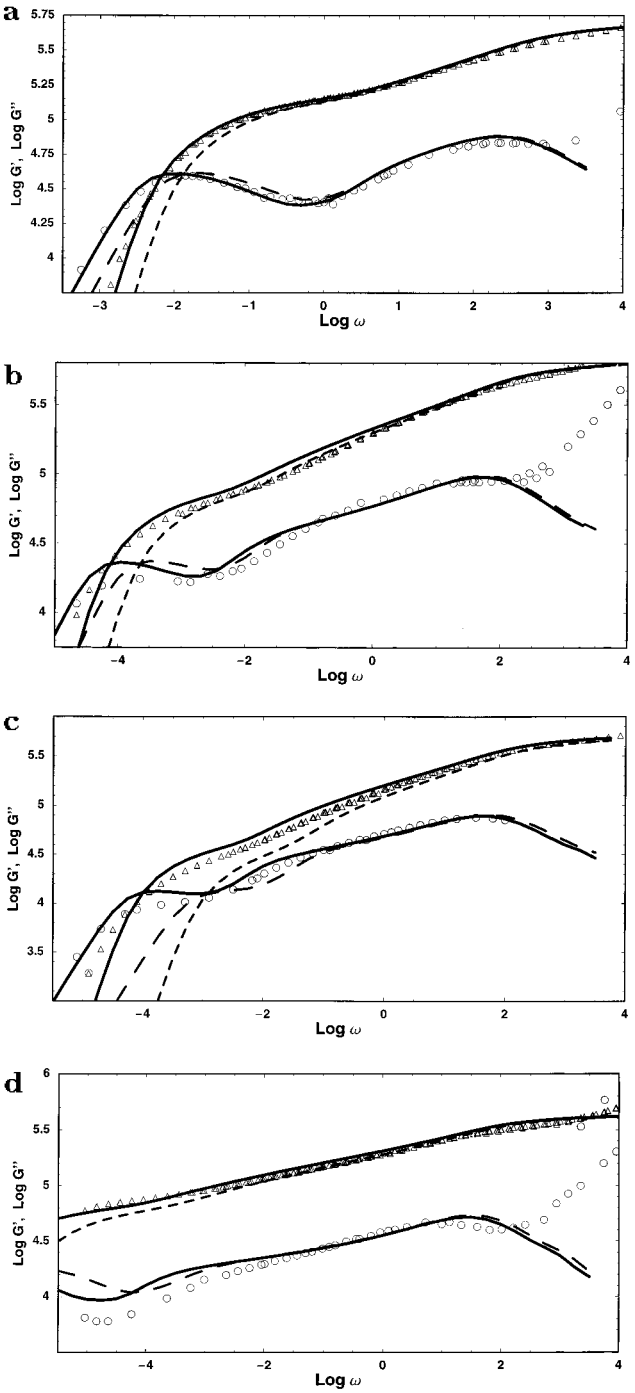

Figure 6. Data and theoretical predictions of $G'(\omega)$ (triangles) and $G''(\omega)$ (circles) for the four H-polymers in this study: (a) H110B20A, (b) H160B40A, (c) H110B52A, and (d) H200B65A. The dashed curves are the theory without any effect of polydispersity, the solid curves use the approach of Appendix C.

relaxation times.[35] Values used for M_e were calculated from direct measurements of plateau modulus and density to allow for small changes in residual solvent content and microstructure between the samples. All values found were in the range reported in the literature of 4000−5000 for 1−4 PI.[11] We found best-fit rheological values for the dimensionless structural parameters $s_a = M_a/M_e$, $s_b = M_b/M_e$, ϵ_a, and ϵ_b in each case. These are compared with the values obtained from synthesis and characterization in Table 2.

It is notable that the more successfully monodisperse the synthesis and fractionation, the more closely do the

Table 2. Comparison of Synthesis and Characterization for Structural Parameters[a]

polymer	s_a(ch)	s_a(fit)	s_b(ch)	s_b(fit)	ϵ_a(ch)	ϵ_a(fit)	ϵ_b(ch)	ϵ_b(fit)
H110B20A	4.1	5.2	22.2	28.9	0.01	0.01	0.13	0.13
H160B40A	8	9.4	33	25.2	0.05	0.03	0.3	0.48
H200B65A	27	16	50	34	0.05	0.02	0.2	0.28
H110B52A*	10.4	10.4	22.2	22.2	0.02	0.026	0.13	0.63

[a] Values for plateau moduli and time scales employed for these samples at 25 °C, and at 90 °C for the nonlinear experiments (see text), are tabulated in Appendix E.

rheologically derived molecular weights and structures match with the chemically targeted values. The "cleaner samples" (H110B20A and H110B52A) are particularly well represented by both the structural parameters and the form of the curves over at least 6 decades of frequency dominated by entangled modes. Naturally the theory described does not capture the high-frequency unentangled Rouse relaxations, although these could be included without additional parameters.[12] The shapes of both principle features of the spectra are well-described, although one common quantitative discrepancy is the overprediction of the minimum in $G''(\omega)$ lying between the arm and cross-bar relaxations. This is not true of the very largest polymer studied, although in this case the longest relaxation times were inaccessible to our oscillatory experiment. This "fill-in" of the spectrum is quite consistent with the calculation of the amplified effect of polydispersity in the arms at just this time scale. The longest relaxation times of the arms in a sample will be spread exponentially in this region of the spectrum. A similar effect is expected and seen as a broadening of the reptation peaks.

Once the shoulder features have been identified with the relaxation distribution of the dangling arms, we are in a position to compare this component of the spectrum with that of the arms of similar molecular weight but belonging to pure PI stars. A suitable collection of such data was presented by Fetters et al.[7] and compared favorably with a tube model theory of Milner and McLeish.[35] A comparison of the two data sets purely by eye affirms that the relaxation times of entangled arms are much longer in the presence of the (effectively fixed) cross-bars. Ignoring prefactors, the main dependence of the longest arm relaxation time on arm molecular weight can be written $\tau_a(1) \approx \tau_e e^{\nu'(\phi_a)s_a}$ Figure 7 shows a plot of experimentally derived values for ν' from the H-polymers in this study, Roovers H-polystyrenes[17] and star PI.[7] Each geometry of H-polymer has a specified ϕ_a independent of molecular weight (e.g., Roovers' H−PI all had $\phi_a = 0.8$ and the star polymers have $\phi_b = 0$). The prediction for the function $\nu'(\phi_a)$ is also shown in Figure 7. The significant impediment the cross-bars present to the process of dynamic dilution is the reason for this variation in the prefactor ν', first observed by Roovers.[17]

4.2. Nonlinear Step Strain. Figure 8 shows the nonlinear relaxation modulus following a series of shear strains on the sample H111B20A. At small strains, the relaxation curve reproduces that of linear response. In the window of time scales available to the experiment at room temperature, the only significant relaxation is that of the cross-bar reptation; the curve is dominated by relaxations of about 300 s. However, at strains of 150% and above, an additional relaxation is apparent in the data at time of order 10 s. Before this time, the response is not as strain thinning as it is at longer time scales, when the strain dependence is similar to the Doi−Edwards form for linear polymers. Estimation of the stretch relaxation time of the cross-bar from eq 14 gives a value of just this order. Also shown on Figure 8 are predictions for $G(t, \gamma)$ calculated from eq 12. The calculations share the features of weaker strain dependence of the stress at earlier times and the emergence of the new nonlinear relaxation times at high strains. Significantly, both theory and experiment agree that the response of this H-polymer melt is not time-strain factorable until after the relatively long time τ_s.

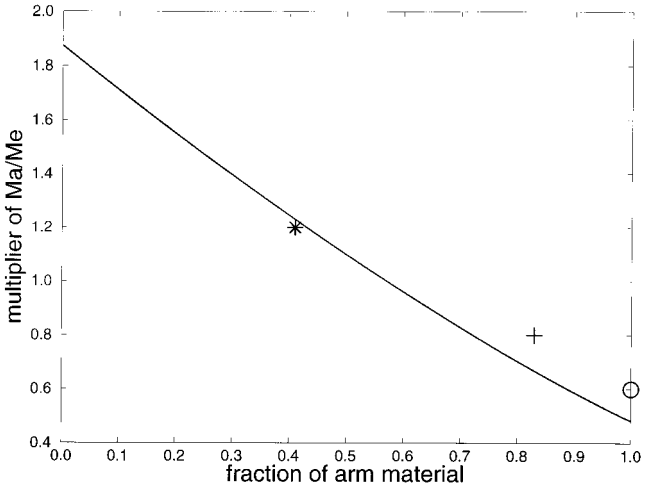

Figure 7. Plot of the predicted prefactor to the arm molecular weight in the exponential term of all long-time dynamical quantities as a function of arm material fraction. Data from Roovers' H-polystyrenes (+), PI star (○), and this study (*) are represented by the three points.

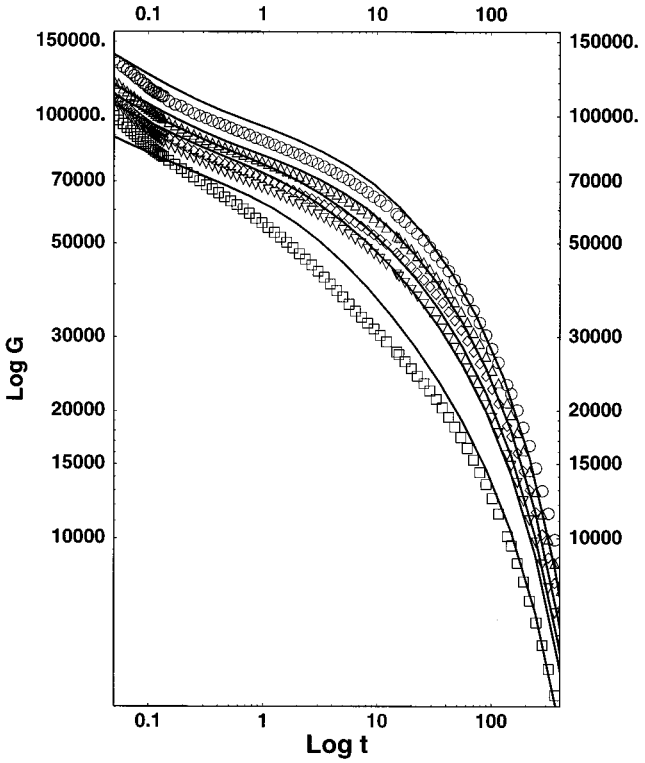

Figure 8. Data and theoretical curves for the relaxation modulus of H110B20A in large-step shear. Strains are 10% (○), 30% (△), 100% (◇), 200% (▽), and 300% (□). Note the increasing magnitude and decreasing time scale of the relaxation process that enters visibly at 200% and above. The units of time are seconds.

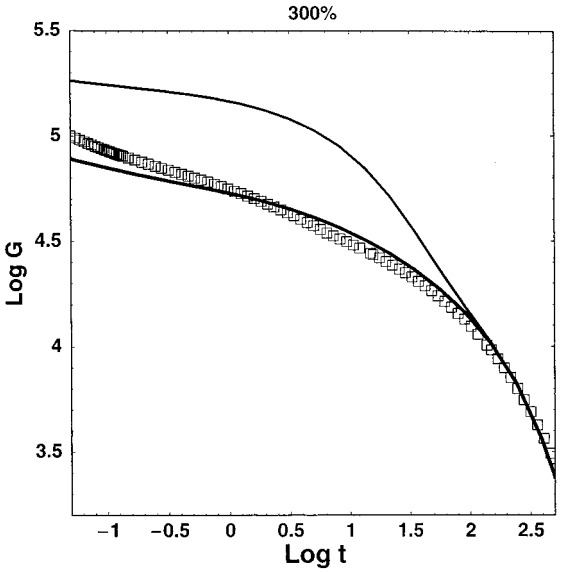

Figure 9. 300% step shear data in comparison with the theory taking a fixed stretch relaxation time (stress independent) and the more refined theory assuming partial branch-point withdrawal (lower curve).

Of course, the quantitative forms of the predicted relaxation curves only attain good agreement with the data for a restricted range of values for the parameter ν^*. In this regard, the data do show good evidence of the strain-dependent stretch relaxation time discussed in section 2. The surprise is the size required for ν^*. The curves of Figure 8 were calculated for $\nu^* = 20$. This is so large that it indicates rather a failure of the quadratic potential to act as a good model for the localization field of the branch point. Yet, a far poorer account of the experiment is given by a cruder theory that keeps a fixed value of τ_s independent of strain (see Figure 9). The dependence of the current relaxation time of the cross-bar stretch on its current level of strain does indeed broaden its spectrum of relaxation times enormously after large strains. The data are consistent with such a strain-dependent broadening: the extra relaxation process is visible in $G(t, \gamma)$ from $t = 1$ *s* at 300% strain but from $t = 0.1$ s at 400% strain. The overly large value needed for intermediate strains results in an underprediction of the stress at early times for strains in excess of 300%. A physical picture consistent with these findings is one in which the branch point is only weakly confined for small strains (so perturbing the stretch relaxation very sensitively), becoming more restricted at higher strains. The corresponding localizing potential would be much flatter than a quadratic function near the mean position of the branch point, but becoming steeper as displacements become large relative to the tube diameter. So, this is one effect for which the predictions of "hard-walled" and quadratic tubes differ markedly. However, this discussion must await the scattering experiments and results on other flows before any firm conclusions may be drawn (see below).

For very large shear strains $\gamma \geq 400\%$, the theory predicts branch-point withdrawal. The main consequence of this is a resumption of strain thinning at times earlier than τ_s. The experiment carried out with an initial strain of 500% does indeed exhibit a weaker initial response, which is consistent with the early-time damping function calculated in eq 11. For higher strains still, the early-time damping function falls off much more rapidly with strain. In Figure 10, we plot the strain dependence of the data in the form of apparent damping functions at both early ($t \ll \tau_s$) and late ($t \gg \tau_s$) times and compare it with the two limiting forms predicted for this architecture. It is apparent that the late-time response is much closer to the Doi−Edwards form (the polymer is effectively linear at these time scales), whereas the early time strain dependence follows the stiffer response predicted to arise from a polymer containing a nonretracting section (in this case, the cross-bar) up to a critical strain of just under 400%.

4.3. Transient Shear and Extension. A further set of nonlinear rheological experiments were made on the sample with the clearest time scale separations, H110B20A. The transient shear stress as a function of time after initiation of the flow was measured for a range of shear rates from linear response to rates of order τ_s^{-1}. The results are given in Figure 11, together with the results of the constitutive predictions of eq 18. The cleanly defined terminal time results in the wide range of (small) shear rates for which the resulting "transient viscosity" is purely that of linear response. When shear rates become of order τ_{rept}^{-1}, a mild overshoot appears in the transient, but this remains small until the shear rate is of order τ_s^{-1}, when it becomes more marked and moves to earlier times (and strains). This is qualitatively similar to the shear transients ascribed to chain stretching in very rapid flows of linear polymer melts. However, in this case, the renormalization of τ_s due to branch-point withdrawal has a strong modifying effect on the strength of the overshoot. Optimization of the corresponding parameter ν^* in this case also indicated highly mobile branch points at the moderate stretches induced by the faster flows, although the best agreement in this geometry was with rather less extreme values than in the large rapid step strains ($\nu^* = 1$ in this case, as one might expect on physical grounds). Without any change of parameters from the case of linear rheology (apart from mild adjustments to G_0 to accommodate typical instrumental variation and the WLF shift to τ_e at 90 °C), both the emergence and size of the overshoot and the steady-state shear thinning are well-described by the theory. This is remarkable given the small number of parameters in the molecular model and the previous constraints set on them. The principle divergence of theory and experiment is the over-early prediction of the precise onset of strong shear thinning as a function of shear rate. This would be less severe if the stretch time were left as a truly free parameter, but we have chosen to constrain it via the theory and step−strain experiments here. In light of the difficulty presented by step−strain experiments for these highly elastic materials, it may prove better practice to rely on transient flow experiments to fix model parameters in the nonlinear case. The most obvious remaining discrepancy is in the exact strain at which the shear-stress maximum occurs in the higher flow rate experiments. The data reach a maximum stress a little later than that predicted by the model. It is possible that this feature arises from a simplifying assumption implicit in the constitutive equation we developed in section 2.[18] In this first treatment, the orientation relaxation times of the cross-bar segments were held at their equilibrium values. However, as orientation develops with strain, so does the relative curvilinear velocity of the tube and cross-bar itself. This not only gives rise to the drag that induces chain stretching but also imposes a local

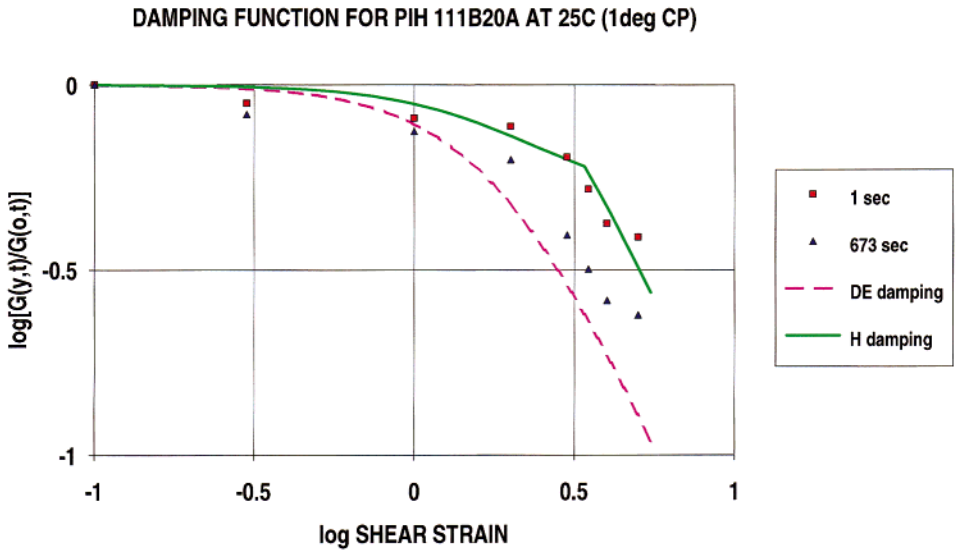

Figure 10. Predicted damping functions at early ($t = 1$ s $\ll \tau_s$) and late ($t = 673$ s $\gg \tau_s$) times together with step shear data from H110B20A. The early-time response is less shear thinning because only the arms, but not the cross-bar, have retracted. Beyond the critical strain for branch-point withdrawal, the damping function follows the Doi−Edwards gradient but lies everywhere above it as the cross-bar retains a stretch of 2. At long times, the response is much closer to the Doi−Edwards form for linear polymers, reflecting the renormalized linear nature of the melt of cross-bars at these time scales.

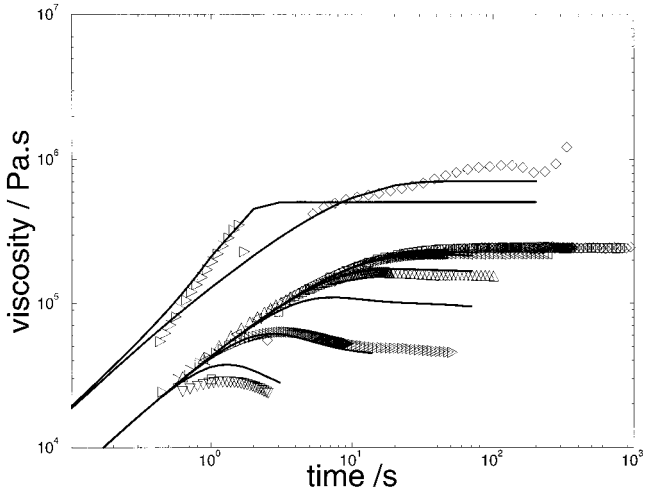

Figure 11. Transient viscosities in shear and extension for H110B20 together with calculations assuming pom-pom constitutive equations supplemented with linear viscoelastic responses from the fast arm and cross-bar extremities, eq 18. Extension rates are 0.03 and 1 s^{-1}. Shear rates are 0.01, 0.03, 0.1, 0.3, 1, and 3 s^{-1}.

deformation rate for segments at the extremities of the cross-bar that is higher than the bulk deformation rate by a factor of order s_b (the local rate is $\sim v_{tube}/a \simeq s_b$ ($\mathbf{K}$: $\langle \mathbf{S}(t, x_b)\rangle_{x_b}$)/$a$). Such an expected renormalization of the local orienting effect of the bulk flow would enhance the stretching peak at strains later than in the present simple theory. However, the effect is rather subtle, and a detailed consideration is left to future work.

In extension, the experiments clearly revealed a qualitative difference in flow type between nonstretching ($\dot{\epsilon}\tau_s < 1$) and stretching ($\dot{\epsilon}\tau_s \geq 1$) flows. The lower rates gave an extensional transient characteristic of the same linear response as the shear experiments (although the measured nominal values of the stress were consistently about 30% higher). As soon as the flow rate entered the stretching regime, the sample behaved more like a rubber than a melt in the extensional rheometer and exhibited rapid and early strain hardening to break. For clarity, we present just one set of results in each flow regime in Figure 11, together with the predicted uniaxial extensional response. The theoretical curves were calculated from the full constitutive eq 18, using precisely the same molecular parameters as those for the shear transients. The quantitative agreement is remarkable. Again a value of $\nu^* = 1$ was consistent with the data. Although the breaking points experienced in the higher stretch-rate experiments were not much higher in stress than the linear response curve (see Figure 11), this is quite consistent with the relatively low critical stretch of the cross-bar for the $q = 2$ H-polymers. Moreover, the breakpoint is a direct prediction of the molecular rheology, as the extension thinning predicted as soon as the cross-bar stretch reaches its maximum value destabilizes the stretching filament. This viscoelastic extension of the "Considère criterion" for filament failure has recently been predicted to occur in the case of pom-pom architectures, such as the H-polymer,[41] and in the context of molecular modeling of LDPE.[42] This is the first time it has been observed in a model polymer.

4.4. Small-Angle Neutron Scattering. The large-strain experiments discussed above strongly support the special deformation of the branch point within the entanglement network suggested by our theory. However, without direct structural information from a technique such as SANS, the evidence is far from conclusive. The logic behind the special deuterium labeling described in section 3 is that, at strains larger than the critical strain for branch-point withdrawal, the pairs of labeled ends actually approach each other on further strain, rather than separate (see Figure 5). Such extremely nonaffine behavior ought to have a clear signature in SANS. This is because the principle RPA peak in the melt scattering is dominated by correlations from pairs of deuterated segments separated by the cross-bar. When branch-point withdrawal occurs, the pairs of labeled ends on the same side of the cross-bar are themselves better correlated spatially. This in turn amplifies the signal from the correlation with their "opposite" pair. Even the small retraction of the free

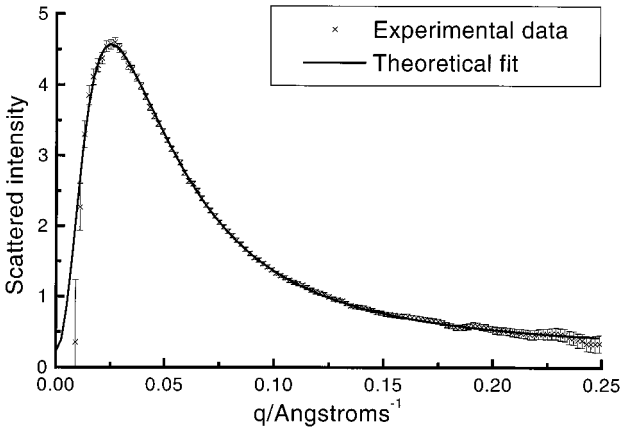

Figure 12. Isotropic melt scattering from the labeled polymer H110B52A together with the RPA prediction. A constant incoherent scattering has been assumed. The scaling for R_g is consistent with literature values for PI.

arms, together with the small shifts of the branch point up to a tube diameter, which we have proposed to explain the nonlinear rheology reported above, would produce strongly nonaffine features.

The first experiment consisted of the important check at zero strain. An isotropic peak in the scattering intensity as a function of wavevector $S(q)$ was observed (see Figure 12). In this case, the theoretical scattering function is straightforward to calculate using the standard random phase approximation, albeit adapted to the special architecture of a H-polymer melt.[36]

$$S(\mathbf{q}) = \frac{S_{AA}(\mathbf{q})S_{BB}(\mathbf{q}) - [S_{AB}(\mathbf{q})]^2}{S_{AA}(\mathbf{q}) + S_{BB}(\mathbf{q}) + 2S_{AB}(\mathbf{q})} \qquad (21)$$

Here, the partial structure factors are calculated from the correlations of the deuterated, hydrogenous, and cross-correlated parts of a single Gaussian H-polymer. The theoretical "RPA peak" is an almost perfect fit to the data, with values for the radius of gyration of PI melt consistent with values toward the lower end of those in the literature (we used a relation between molecular weight and radius of gyration such that for a linear PI melt, $R_g = 0.298(M_{PI})^{1/2}$. Although RPA peaks are never highly structured, the result would have been significantly different for, say, a linear triblock of the same overall dimensions. This is therefore another experimental confirmation of the synthesis as designed.

The interpretation of the scattering patterns from the stretch and quench experiments is much less straightforward, however. The standard RPA theory can no longer be used because the melt is no longer at equilibrium. To predict the effect of the tube on the bulk scattering, one of us (D.J.R.) has developed an extension to the RPA theory that respects two types of variables: the quenched and strained configurations of unrelaxed tube constraints and the annealed variables describing coordinates of chains that have been free to relax to a local equilibrium before the temperature quench.[37] An outline of the method is given in Appendix D. Figure 13 shows the experimental and theoretical scattering obtained from an extensional stretch of 2.3. The pattern is clearly highly anisotropic and very different from an affine deformation. There is a very pronounced enhancement of the RPA peak in the direction of the stretch and a weakening in the perpendicular direction. Now at this stretch, we do not expect the branch point to be withdrawn far into the tube of the cross-bar, but a significant displacement of the order of the tube diameter is likely if the localizing potential for the branch point is sufficiently flat (see discussions in the theory section preceding equation 16). In Figure 14 we compare the curves of scattered intensity parallel and perpendicular to the stretch with calculations assuming (i) no arm retraction at all, (ii) arm retraction but no disequilibration of the branch point, and (ii) retraction of the branch point by just one tube diameter. Although none of the three assumptions gives an exact fit to the scattering, the last is by far the best. No further retraction is able to explain the remaining discrepancy in the peak heights. It may arise from an effect known to exist in polymer networks under strain but never as yet observed in polymer melts − elastic inhomogeneities. Apart from any contour retraction, as we expect in branched melts, the existence of spatial variation in cross-link density has recently been invoked to explain the "butterfly" scattering patterns from stretched, partially labeled networks.[38] A mobile component of the network swells regions of low cross-link density on strain. As the scattering patterns in this case are similar to those observed in our experiment, a similar inhomogeneity in the instantaneous entanglement density would indeed enhance the observed peak beyond the level predicted by retraction and partial branch-point withdrawal alone. A second intriguing possibility is that the underprediction of the strong parallel peak is simply due to the preaveraging approximation in which each chain is assumed to sample uniformly all possible orientations along its contour. This works well for rheology even for moderately entangled chains but may be far less accurate for scattering. This is because strong scattering in any direction at the peak is due to chains that already have an orientational bias in that direction. If this is the stretch direction, branch-point withdrawal will commence at smaller than average strains, leading to enhanced scattering. Work to evaluate this effect is in progress.

Taken together, the SANS and nonlinear rheology provide a clearer picture of the local configuration of the branch points controlling the slow linear and nonlinear dynamics of the H-polymer melts. If the harmonic localizing potential $U_{loc}(s)$ is assumed, then for a displacement of the branch point of a at the bulk strains of the SANS experiments, the range of the potential w^2 has a lower bound of 3 in our dimensionless units. This is quite consistent with the values of ν^* rather larger than unity needed to explain the rheological experiments and supports the conjecture that the high mobility of branch points in their local entanglement structure is a strong moderator of melt rheology. If the difficult step−strain experiments are given as much weight as the transient flow results, then the different effective localizing potential required in each case indicates that there might be strong local effects depending, at least indirectly, on the rate of deformation. All strains were achieved within 0.1 s in the step−strain experiments, much faster than even the highest transient deformation rates. An experiment to test this conjecture would be a much more controlled SANS measurement on samples carefully quenched after stretching at different rates.

5. Conclusion

We have undertaken a systematic experimental study over a wide range of time scales of the dynamics of

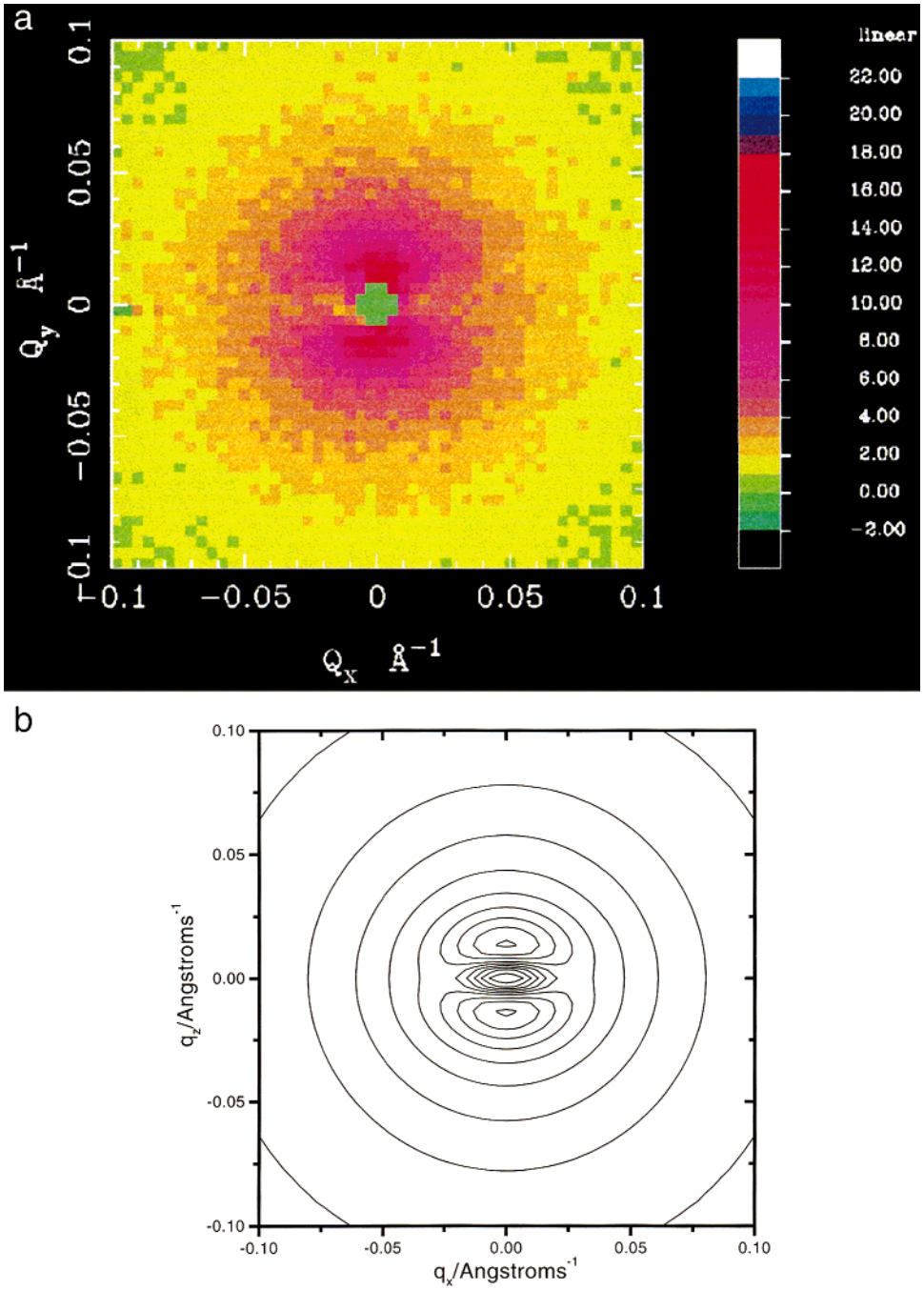

Figure 13. Observed and predicted 2-D scattering plots from H110B52A on quenching rapidly from an affine extensional strain of 2.3. About half of the arm material is calculated to have relaxed before the quench.

entangled H-polymers, using both rheology and neutron scattering to probe the molecular processes underlying the unusual dynamics of this branched polymer. At every point, we have used our data to evaluate the techniques currently available for treating the tube model of polymer melts. When evaluated in the light of theory, the data on our model systems point to several important aspects of the physics of branched polymers with greater complexity than simple stars.

The linear rheology is well-accounted for by the assumption of path-length retraction in the dangling arms, followed by reptation/fluctuation of the cross-bar. In these clean and highly entangled systems, both processes are well-resolved in time scale. The presence of the cross-bar has several important consequences for the relaxation of the dangling arms. First, their presence as unrelaxed material during the faster dynamics of the arms greatly slows the arm retraction relative to the rate it would adopt in a melt of pure stars. The coefficient of M_a/M_e in the exponential term for all long time scales increases with the fraction of cross-bar material. Second, the presence of this effectively fixed network fraction enhances the role of polydispersity in the arm molecular weight. The presence of even the small degree of polydispersity arising in anionic polymerizations shifts the terminal time of the retracting arms to a longer time scale than that which would result from a monodisperse ensemble possessing the same weight-average molecular weight. This is another important difference from pure star melts, which do not have this property.

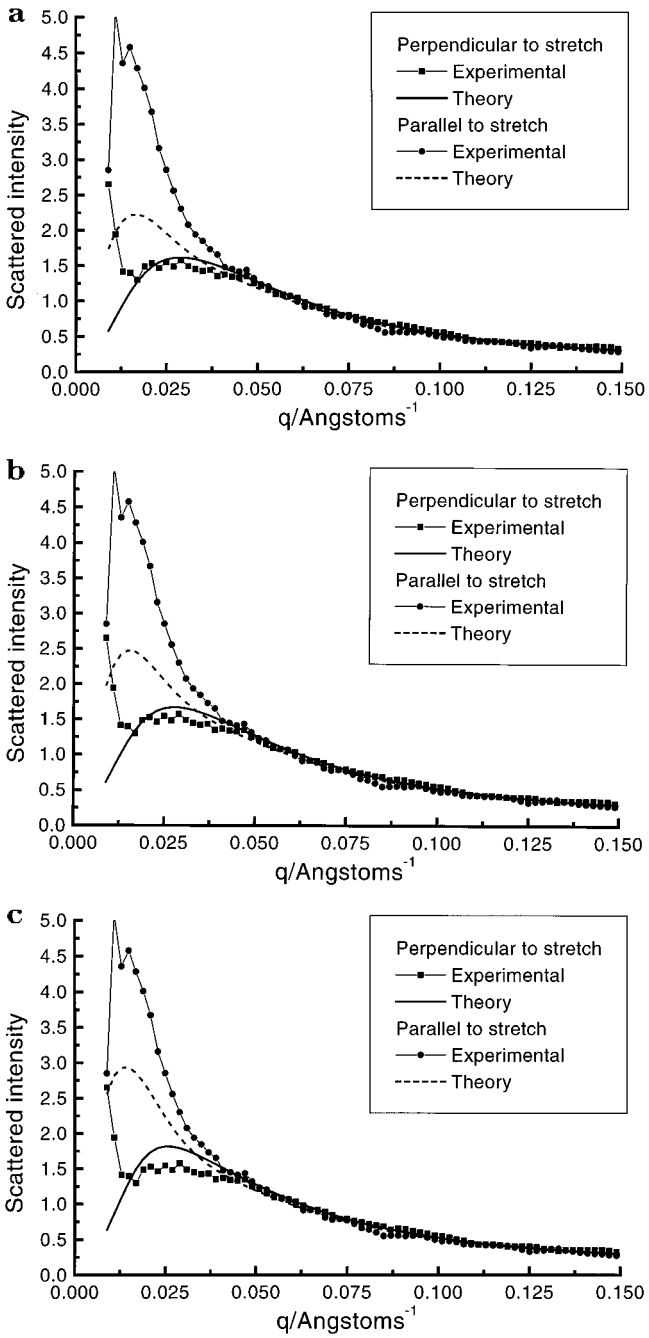

Figure 14. Predicted scattering intensity parallel (dashed) and perpendicular (solid) to the stretch direction together with data on H110B52A after the 2.3 extensional strain: (a) assuming no retraction of arm or cross-bar, (b) assuming arm retraction only, and (c) assuming partial withdrawal of the branch points into the cross-bar tube by one tube diameter.

In nonlinear deformation, the predictions of earlier tube model calculations for branched polymers have been confirmed, with the suggestion of some important refinements. In particular, a melt of H-polymers does not show time-strain factorability for all times later than the pure Rouse time of the chains, as is the case in linear polymer melts. Instead, a new relaxation time arises that separates the later Doi−Edwards dependence on strain with an earlier, stiffer response. We have identified this relaxation mode with the curvilinear stretch relaxation of the cross-bar, dragging against the renormalized friction of the branch points. This interpretation is not quantitatively consistent with a branch-point friction independent of stretch but lends support to a dependence on strain of the local configuration of the three chains meeting at the branch point. Increased tension in the cross-bar tends to shorten the entangled path length of the dangling arms by withdrawing them slightly into the cross-bar tube. Because of the exponential dependence of the branch-point friction on the dangling path length of the arms, this can modify the stretch relaxation strongly. At larger strains, complete withdrawal of the arms into the cross-bar tube is consistent with the much larger strain thinning above shears of 500%.

The progressive branch-point withdrawal process was also indicated by SANS experiments on elongated and quenched samples of selectively deuterated H-polymers. Significant displacement of the branch points within the tube constraints of up to 1 tube diameter, even before the critical strain for complete withdrawal, is suggested by the amplification of the main scattering peaks away from the purely affine prediction. Further scattering experiments of this kind are suggested by the results and by the newly developed extension of RPA theory capable of interpreting melt scattering from labeled polymers of complex architecture.

All of these features showed up equally in transient flows in both shear and extension. The stretch relaxation gave rise to strong shear-stress overshoots at high strain rates. Although very difficult to perform with such elastic materials in small quantities, the extensional measurements were able to confirm the prediction of rapid hardening to break at high extension rates.

Our results show that recent predictions of the rheological response of the H- and generalized pom-pom architectures conjectured on the basis of the tube model[21] are essentially correct, but with an even greater sensitivity to strain in the mobility of branch points. The molecular phenomenon of branch-point withdrawal underlies all of the nonlinear phenomena we examined. This suggests that the excellent processing characteristics of randomly long-chain-branched polymers result in part from an ability to adapt their intrinsic relaxation times to the flow constraints imposed upon them.

There is a strong need to develop studies of this kind on more highly branched architectures and on controlled blends. Scattering both on quenching and in the steady-state will certainly continue to complement rheological data as the molecular models are continually developed.

Acknowledgment. Financial support from EPSRC (U.K.), the E.U., BP Chemicals plc, Corning Cable plc, and Smith and Nephew plc is gratefully acknowledged. We thank O. G. Harlen, R. G. Larson, S. T. Milner, and M. Rubinstein for helpful discussions.

6. Appendices

A. Linear Stress Relaxation. The time-dependent modulus is calculated for the melt of H-polymer as a sum of contributions from each segment along the arms and the backbone. The dynamic modulus $G^*(\omega)$ is related by Fourier transform to the time-dependent modulus (see eq 2 in section 2) as $G^*(\omega) = i\omega F[G(t)](\omega)$ and is obtained as

$$G^*(\omega) = G_0(\alpha + 1) \times \left[\int_0^1 \mathrm{d}x_a \phi_a (1 - \phi_a x_a)^\alpha \frac{i\omega\tau_a(x_a)}{1 - i\omega\tau_a(x_a)} + \int_0^1 \mathrm{d}x_b \phi_b^{\alpha+1} (1 - x_b)^\alpha \frac{i\omega\tau_b(x_b)}{1 - i\omega\tau_b(x_b)} \right] \quad (22)$$

where $\tau_a(x_a)$ and $\tau_b(x_b)$ are the characteristic times of arms and backbone relaxation at the segment x_a and x_b, respectively. The shear storage modulus $G'(\omega)$ and shear loss modulus $G''(\omega)$ are the real and imaginary parts of $G^*(\omega)$ in eq22, respectively. The shear storage modulus is obtained as

$$G'(\omega) = G_0(\alpha+1)\times \left[\int_0^1 dx_a \phi_a(1-\phi_a x_a)^\alpha \frac{\omega^2\tau_a(x_a)^2}{1+\omega^2\tau_a(x_a)^2} + \int_0^1 dx_b \phi_b^{\alpha+1}(1-x_b)^\alpha \frac{\omega^2\tau_b(x_b)^2}{1+\omega^2\tau_b(x_b)^2}\right] \quad (23)$$

The shear loss modulus is obtained as

$$G''(\omega) = G_0(\alpha+1)\times \left[\int_0^1 dx_a \phi_a(1-\phi_a x_a)^\alpha \frac{\omega\tau_a(x_a)}{1+\omega^2\tau_a(x_a)^2} + \int_0^1 dx_b \phi_b^{\alpha+1}(1-x_b)^\alpha \frac{\omega\tau_b(x_b)}{1+\omega^2\tau_b(x_b)^2}\right] \quad (24)$$

A.1. Arm Relaxation. At shorter time scales (high-frequency dynamics), arm retraction faces a barrier of less than k_BT, and we estimate the relaxation rate from these small retractions by studying the motion of the end of a semi-infinite Rouse chain in tube. The arms' free ends retract partway within their tubes and poke out along a new direction and thus renew only part of the arm conformation near the free end. These early fast (diffusive) fractional displacements are the same as those in star polymer arms, and the characteristic time is $\tau_e(x_a)$ (see eq 3 in section 2). These relaxation processes cross over to the activated retraction at a time on the order of the Rouse time of the arm.

For larger values of x_a or longer times, arm retraction is entropically unfavorable and hence activated. Thus, there is a free energy barrier to retract that is increasingly larger for deeper retractions. The potential barrier $U_{a\ eff}(x_a)$ for retraction of a fractional distance x_a ($0 < x_a < 1$) down the tube for a arm in a fixed network of entanglements is[31]

$$U(x_a) = ({}^{15}/_{8})s_a x_a^2 \quad (25)$$

where s_a is the entangled path lengths of the arms. The barrier to full retraction $U(1)$ is exponential in s_a, which leads to very long terminal times for arms and a very broad spectrum of relaxation times corresponding to partial arm retraction; i.e., the arm segments with $x_a' < x_a$ have relaxed many times over, whereas arm segments $x_a' > x_a$ with volume fraction $\Phi(x_a) = \phi_b + \phi_a(1-x_a) = 1 - \phi_a x_a$ are effective at topologically confining segments at x_a. All faster-relaxing material is regarded as absent from the entangling network on time scale $\tau_a(x_a)$. This dynamic dilution speeds up the arm retraction in melt as compared to a arm retraction in a fixed network. The recent scaling theory[10] as well as experiments on the plateau moduli in theta-solution,[9] imply that the diluted modulus scales as

$$G(\Phi(x_a)) = G_0\Phi(x_a)^{1+\alpha} \quad M_e(\Phi(x_a)) = M_{e0}/\Phi(x_a)^\alpha \quad (26)$$

with $\alpha = {}^4/_3$. The time scale $\tau_a(x_a)$ for the retraction of a fractional distance x_a ($0 < x_a < 1$) down the tube sets the attempt frequency for retraction to $x_a + \Delta x_a$, and the potential difference $U(x_a + \Delta x_a) - U(x_a)$ sets the barrier for it. In the differential limit this becomes[8]

$$\frac{\partial U(x_a; M_e(x_a))}{\partial x_a} = \frac{dU_{a\ eff}(x_a)}{dx_a} \quad (27)$$

The solution of eq 27 ($U_{a\ eff}(x_a)$) is

$$U_{a\ eff}(x_a) = \frac{15 s_a}{4}\frac{1-(1-\phi_a x_a)^{\alpha+1}(1+(1+\alpha)\phi_a x_a)}{(1+\alpha)(2+\alpha)\phi_a^2} \quad (28)$$

We obtain the characteristic relaxation time $\tau_{al}(x_a)$ by solving a first-passage time problem, considering the arm free end as a random walker with diffusion coefficient $D_{a\ eff}$ in the potential $U_{a\ eff}(x_a)$. The first-passage time is given by[8]

$$\tau_{a\ l}(x_a) = \frac{L_a^2}{D_{a\ eff}}\int_0^{x_a} ds' \exp[U_{a\ eff}(s')]\int_0^{s'} ds'' \times \exp[-U_{a\ eff}(s'')] \quad (29)$$

where L_a is the primitive path length of arm corresponding to the proper square end-to-end distance $R_a^2 = N_a b^2$ and $L_a a = R_a^2$. The effective diffusion coefficient of arm for the purposes of retraction is $D_{a\ eff} = 2D_R$ with $D_R = k_BT/N_a\xi_0$. ξ_0 is the monomer friction coefficient, related to Rouse relaxation time as $\tau_R = \zeta_0 N_a^2 b^2/(3\pi^2 k_B T)$. The ratio $L_a 2/D_{a\ eff}$ is equal to $(15\pi^2/8)s_a\tau_R$.

For large s_a and finite x_a, the outer exponential factor becomes very large and the integral over s' is dominated by the region near x_a. The inner integral, approximately extended to all s'', is dominated by the region near $s'' = 0$ and can be approximated by $[\pi/2U_{a\ eff}''(x_a = 0)]^{1/2}$. The asymptotic value of the above integral for x_a away from 1 (the potential has finite slope) is

$$\tau_{a\ l}(x_a) = \frac{L_a^2}{D_{a\ eff}}\frac{\exp[U_{a\ eff}(x_a)]}{U_{a\ eff}'(x_a)}\left(\frac{\pi}{2U_{a\ eff}''(x_a=0)}\right)^{1/2} \quad (30)$$

where $U_{a\ eff}'(x_a) = 15 s_a x_a(1-\phi_a x_a)^\alpha/4$ and $U_{a\ eff}''(x_a = 0) = 15 s_a/4$.

The small x_a (early-time) and large x_a (late-time) results are interpolated as for star[8] and linear[12] polymers using a weighted harmonic mean of the two characteristic time behaviors. The simple crossover formula is

$$\tau_a(x_a) = \frac{\tau_e(x_a)\exp[U_{a\ eff}(x_a)]}{1+\tau_e(x_a)\exp[U_{a\ eff}(x_a)]/\tau_{al}(x_a)} \quad (31)$$

This simple crossover form works because $\tau_a(x_a)$ goes as $\tau_{a\ e}(x_a)$ for small x_a because $U_{a\ eff}(x_a)$ and $\tau_{a\ e}(x_a)/\tau_{al}(x_a)$ goes to zero. Similarly, $\tau_a(x_a)$ goes as $\tau_{al}(x_a)$ as $\tau_{a\ e}(x_a)\exp[U_{a\ eff}(x_a)]/\tau_{al}(x_a) \gg 1$ for intermediate values of x_a.

A.2. Backbone Relaxation. On time scales greater than $\tau_a(1)$, the dynamics are controlled by H-polymer crossbar material as the arm material is already relaxed. The long-time behavior of the H-polymer is similar to that of a linear polymer with all of the friction confined to the branch point. Though earlier studies considered that linear (and so linear-like) polymers relax by the reptation mechanism alone, recent studies[12] and this work suggest that linear polymers exploit the fast retraction

modes of relaxation as a two arm star at earlier time scales than the reptation time. The main difference between star and backbone H-polymer stress relaxation is that the retraction in cross-bar relaxation is cut off by its reptation.

In the framework of the tube model, configurational rearrangements of the backbone are accomplished by two means: (i) (early-time) fast retraction of the effective free ends (branch points) of the H-polymer cross-bar back and forth along its contour with random choice of new paths and followed by (ii) reptation of the cross-bar (in a diluted virtual tube) back and fourth along its contour with random choice of new paths so that the original virtual tube "dissolves". The idea behind the combined relaxation mode is simple because the pure reptation modes of relaxation allow very slow modes of relaxation but the inclusion freed branch-point fluctuations on shorter time scales enhance the tube dissolution and hence offer a faster route to relaxation to material near the extremities of the entangled path length.

The diffusion coefficient of the branch points is calculated as the distance moved by a branch point (which will be on the order of the current tube diameter $a_{b\ eff}$) after the residence time of completely retracted state $\tau_a(1)$, so $a_{b\ eff}^2 \simeq 2D_{b\ eff}\tau_a(1)$. But the effective (retraction) diffusion coefficient should also account for the number of dangling entangled arms, q, on the friction blob. Moreover, only a fraction of diffusive hops in the melt will amount to steps along the tube contour itself. The effective fraction could be estimated by considering that the diffusion is taking place in a three-dimensional lattice of some effective coordination number and a lattice point separation of $a_{b\ eff}$. However it seems more appropriate to introduce an order-one, dimensionless constant (we call it p) representing the fraction of a tube diameter corresponding to each elemental diffusive step of a branch point. Because the drag on the branch point reduces in proportion to the number of arms, we write finally:

$$D_{b\ eff} = \frac{p^2 a_{b\ eff}^2}{2q\tau_a(1)} \tag{32}$$

We will find that a value of $p^2 = {}^1/_6$ accounts well for the rheological data, and we use this value in the following. A number of this order is not at all surprising physically, because of the reduced diffusion constant expected when projecting spatial onto curvilinear motion. Of course $D_{b\ eff}$ decreases exponentially with arm molecular weight.

The idea behind retraction is to treat the cross-bar as two-arm star of arm length of $N_b/2$ where star arm retraction is similar to the contour-length fluctuation. The small fluctuations of freed branch points in two-arm stars of primitive path length $L_b/2$ are given as

$$\tau_{b\ e}[x_b] = \frac{(x_b L_{b\ eff}/2)^2}{2D_{b\ eff}} \tag{33}$$

Substituting values of $L_{b\ eff}$, $D_{b\ eff}$ and replacing $L_{b\ eff}/a_{b\ eff} = 5s_b\phi_b^{\alpha/2}/4$ (obtained by combining $R_b^2 = N_b b^2/2 = L_{b\ eff}a_{eff}$ and $a_{eff}^2 = ({}^4/_5)N_e b^2/\phi_b^{\alpha}$, we obtain

$$\tau_{b\ e}[x_b] = \frac{75}{32} q s_b^2\, \phi_b^{2\alpha} \tau_a[1] x_b^2 \tag{34}$$

For larger values of x_b, branch-point retraction is entropically unfavorable and hence activated. The potential barrier $U_{b\ eff}(x_b)$ for retraction of a fractional distance x_b ($0 < x_b < 1$) down the tube for a backbone in a fixed network of entanglements is[31]

$$U(x_b) = ({}^{15}/_{16}) s_b x_b^2 \tag{35}$$

where s_b is the entangled path lengths of the backbone of the molecule. The effective potential in differential limit is related to eq 35 as[31]

$$\frac{\partial U(x_b;\, M_e(x_b))}{\partial x_b} = \frac{\mathrm{d}U_{b\ eff}(x_b)}{\mathrm{d}x_b} \tag{36}$$

The effective activation potential is obtained by solving eq 36 for $M_e(\Phi(x_b)) = M_{e0}/\Phi(x_b)^{\alpha}$ and $\Phi(x_b) = \phi_b(1 - x_b)$. Hence, the effective potential for the backbone for large x_b retraction (for the star arms of length $N_b/2$) is obtained as

$$U_{b\ eff}[x_b] = \frac{15 s_b \phi_b^{\alpha}}{8} \frac{1 - (1 - x_b)^{\alpha+1}(1 + (1 + \alpha)x_b)}{(1 + \alpha)(2 + \alpha)} \tag{37}$$

Similar to the problem of large x_b ($0 < x_b < 1$) arm dynamics, we obtain the mean first-passage time for the branch points as a random walker with diffusion coefficient $D_{b\ eff}$ and primitive path length $L_b/2$:

$$\tau_{b\ l}(x_b) = \frac{L_b^2}{4D_{b\ eff}} \int_0^{x_b} \mathrm{d}s' \exp[U_{b\ eff}(s')] \int_0^{s'} \mathrm{d}s'' \times \exp[-U_{b\ eff}(s'')] \tag{38}$$

Equation 38 for large $s_b\phi_b^{\alpha}$ and finite x_b can be simplified as

$$\tau_{b\ l}(x_b) = \frac{L_b^2}{4D_{ret}} \frac{\exp[U_{b\ eff}(x_b)]}{U'_{b\ eff}(x_b)} \left(\frac{\pi}{2U''_{b\ eff}(x_b = 0)}\right)^{1/2} \tag{39}$$

where $U'_{b\ eff}(x_b) = 15 s_b \phi_b^{\alpha} x_b (1 - x_b)^{\alpha}/8$ and $U''_{b\ eff}(x_b = 0) = 15 s_b \phi_b \alpha/8$.

The small x_b and large x_b retraction characteristic relaxation times results are interpolated using a weighted harmonic mean scheme which faithfully replicates behavior in the two extremes:

$$\tau_{b\ ret}[x_b] = \frac{\tau_{b\ e}[x_b] \exp[U_{b\ eff}[x_b]]}{1 + \tau_{b\ e}[x_b] \exp[U_{b\ eff}[x_b]]/\tau_{b\ l}[x_b]} \tag{40}$$

The $\tau_{b\ ret}[x_b]$ keeps growing with x_b, and beyond $x_b = x_c$, retraction becomes slower than reptation so that most of the remaining chain segments will relax their stress by reptation at time τ_{rep}.

The reptation relaxation time of the H-polymer cross-bar in a dilated tube is shorter than the deeper retraction time of backbone (τ_{ret}) of the dilated (reduced) primitive path length $L_b(1 - x_c)$ and the effective curvilinear diffusion constant for reptation D_{rep} is[2]

$$\tau_d = \frac{L_{b\ eff}^2 (1 - x_c)^2}{\pi^2 D_{rep}} \tag{41}$$

τ_d is therefore the diffusion time of two one-dimensional walkers of diffusion constant (D_{rep}) for branch points of the backbone to traverse a mean-square distance of L_b^2-

$(1 - x_c)^2$. The collective diffusion constant (D_{rep}) of two random walkers (friction blobs) connected by an entropic spring is calculated for the reptation of these two coupled random walkers. A simple addition of drags from each of the two branchpoints would suggest $D_{rep} = D_{b\ eff}/2$. Substituting values of L_b and D_{rep} in eq 41 and replacing $L_{b\ eff}/a_{eff} = 5s_b\phi_b^\alpha/4$ (obtained by combining $R_b^2 = N_b b^2 = L_b a_{eff}$ and $a_{b\ eff}^2 = (^4/_5)N_e b^2/\phi_b^\alpha$), we obtain

$$\tau_{rep} = \frac{75(1 - x_c)^2 s_b^2 \phi_b^{2\alpha} \tau_a[1] q}{2\pi^2} \tag{42}$$

τ_{rep} is shortened as the retraction has already relaxed the part of contour length of backbone. The fractional retraction−reptation crossover length (x_c) is obtained using the following self-consistent equality:

$$\tau_{rep} = \tau_{b\ ret}[x_c] \tag{43}$$

which together with eqs 40 and 42 define τ_{rep} and give an implicit equation for x_c.

Finally, we construct a crossover form from the backbone retraction (40) to reptation time result (42) as

$$\tau_b[x_b] = \begin{cases} \tau_{b\ ret}[x_b] & x_b < x_c \\ \tau_{rep} & x_b \geq x_c \end{cases} \tag{44}$$

so that all cross-bar segments relax their orientation by the fastest process available to them.

B. Dynamics of Stretch. We develop an expression for the characteristic nonlinear shear relaxation modulus in monodisperse H-polymer melts when it is subjected to a step strain. The H-polymer is the simplest model for which this nonlinear elastic response is relevant, the backbone is capable of being stretched between pinned branch points at either end.

In equilibrium, the criterion of Gaussian chain statistics within the tube model implies that there is a net Brownian force of $3kT/a$ acting on the free end of each chain. Now, if a step strain is applied on it, the backbone unable to reptate (anchored by two branch points on the either ends) stretches affinely. The free arms undergo starlike relaxation modified by the presence of the fixed backbone. The backbone continues to stretch with the further increase of strain until it sustains a maximum entropic tension of $6kT/a$. If the strain increases beyond this critical value, the force balance within the tube is destroyed and the backbone reduces its stretch by sucking the free arms into its tube. This requires continuous reorientation of the sections of arms adjacent to the branch point. At this time scale, the H-polymer may be viewed in terms of a dumbbell model with a stretched backbone attached to a friction blob at either end. We expect the effective friction constants ($\zeta_{b\ eff}$) of the blobs in the nonlinear regime to have the same dependencies on cross-bar fraction, q and a as the branch-point drag to $\zeta_b = kT/D_{b\ eff}$ of the linear regime. However, when branch-point withdrawal is entropically favored, it drastically reduces the friction constants of the branch points and in consequence the relaxation time for tube orientation. The effective friction constant for this rapid withdrawal dynamics is given by

$$\zeta_{b\ eff}(\lambda) = \zeta_{b\ eff} \exp[-\nu^*(\lambda(t) - 1)] \tag{45}$$

where the dimensionless stretch parameter $\lambda(0) = L/L_0$. The constant ν^* contains both the dimensionless prefactor of M_a/M_e in the exponential factor for time scales and the new physics of the potential that localizes the branch point at the meeting point of the tubes around the cross-bars and the dangling arms. A harmonic localizing potential gives rise to the exponential dependence of $\zeta_{b\ eff}$ on λ. The weaker the localizing potential, the larger is the value of ν^*.

The microscopic dynamics of backbone stretch is governed by the balance of two opposing forces: (i) the frictional drag force arising from the relative velocity of the separation of the branch points along the backbone tube and (ii) the Gaussian elastic force tending to restore the backbone to its equilibrium length L_0. Equating these two forces we write,

$$(^1/_2)\zeta_{b\ eff}(L)\frac{\partial L}{\partial t} = \frac{3kT}{a} - \frac{3kTL}{N_b b^2} \tag{46}$$

where N_b is the length of the backbone of the H-polymer. Substituting for ζ_b, $\lambda(0)$, and the tube diameter $a^2 = {}^4/_5 N_e b^2$, (N_e is the entanglement path length), eq 46 can be recast in form of a nonlinear differential equation for $\lambda(t)$:

$$\frac{\partial\lambda(t)}{\partial t} = \frac{(\lambda(t) - 1)}{\tau_s} \exp[\nu^*(\lambda(t) - 1)] \tag{47}$$

and the characteristic stretch relaxation time scale τ_s is given by

$$\tau_s = 5s_b\phi_b^\alpha\tau_a(1) \tag{48}$$

We assume that the localizing potential $U_{loc}(s)$ against branch-point withdrawal is harmonic given by

$$U_{loc}(s) = q\frac{kTs^2}{(wa)^2} \tag{49}$$

so that the dimensionless width of the potential is given by w. This harmonic regime will be valid until branch-point withdrawal occurs at constant force beyond the critical cross-bar stretch q. On stretching the cross-bar to smaller stretches, the branch point displaces so that its tension $3kT(\lambda - 1)/a$ and the localizing force $\partial U_{loc}(s)/\partial s$ balance. The corresponding path-length withdrawn from the arms reduces the effective branch-point friction via the exponential term of eq 30. This gives a final expression for ν^* of

$$\nu^*(\phi_a) = \frac{9}{2}\left(\frac{w^2}{q}\right)\frac{1 - (1 - \phi_a)^{\alpha+1}(1 + (1 + \alpha)\phi_a)}{(1 + \alpha)(2 + \alpha)\phi_a^2} \tag{50}$$

Equation 47 is the time evolution equation for stretch for nonlinear retraction dynamics. For small stretch, this equation can readily be solved by linearizing the exponential and considering up to first-order terms in stretch. This simplifies eq 47 to the following form:

$$\frac{dz}{z(1 + \nu^* z)} = \frac{dt}{\tau_s} \tag{51}$$

Table 3. Coefficient of Expansion A_n

A_1	1
A_2	1
A_3	5/4
A_4	31/18
A_5	361/44
A_6	4537/1200
A_7	757 517/129 600
A_8	2 922 187/317 520
A_9	41 478 457/2 822 400
A_{10}	3 255 225 203/137 168 640
A_{11}	2 652 290 261 711/68 584 320 000
A_{12}	29 273 706 104 263/461 039 040 000
A_{13}	6 268 818 642 766 711/59 750 659 584 000
A_{14}	1 257 201 118 413 824 699/7 212 758 192 640 000
A_{15}	853 066 845 733 489 897/2 932 119 774 904 320

where $z(t) = (\lambda(t) - 1)$ and $z_0 = (\lambda(0) - 1)$. Solving for $z(t)$ and $\lambda(t)$, we have

$$z(t) = \frac{\dfrac{z_0}{1 + \nu^* z_0}\exp(-t/\tau_s)}{1 - \dfrac{\nu^* z_0}{1 + \nu^* z_0}\exp(-t/\tau_s)} \tag{52}$$

and

$$\lambda(t) = 1 + \frac{\dfrac{z_0}{1 + \nu^* z_0}\exp(-t/\tau_s)}{1 - \dfrac{\nu^* z_0}{1 + \nu^* z_0}\exp(-t/\tau_s)} \tag{53}$$

This proves to be a tolerable approximation of the nonlinear dynamics up to initial cross-bar strains of 150% (bulk strains of approaching 300%), but for larger strains, this perturbative approach is not valid. In this case, we directly solve the integral equation for z

$$\int_{z_0}^{z} \frac{\exp(-\nu^* z)}{z}\,dz = -\frac{t}{\tau_s} \tag{54}$$

to get

$$-\gamma_E - \ln(\nu' z) - \sum_{n=1}^{\infty} \frac{(-1)^n(\nu^* z)^n}{n n!} = E_1(\nu^* z_0) + t/\tau_s \tag{55}$$

Exponentiating this expansion, expanding it near $z = 0$, and inverting this series, we obtain

$$z(t) = \frac{1}{\nu^*}\sum_{n=1}^{\infty} A_n \lambda_0^n \exp(-nt/\tau_s) \tag{56}$$

where $\lambda_0 = \exp(-\gamma_E - E_1(z_0\nu^*))$, $\gamma_E = 0.577\,215\,664\,9$ (Euler's γ), and $E_1(z_0\nu^*)$ is the exponential integral defined by

$$E_1(\nu' z_0) = \int_1^{\infty} \frac{\exp(-\nu^* z_0 p)}{p}\,dp \tag{57}$$

The coefficients of expansion A_n in eq 10 are shown in Table 3. The first fifteen terms of the expansion give excellent convergence for an arbitrary value of step strain, with the contribution of the higher order terms becoming significant at smaller times (initially). Consequently, the value of $\lambda(t)$ can be calculated as

$$\lambda(t) = 1 + \frac{1}{\nu^*}\sum_{n=1}^{\infty} A_n \lambda_0^n \exp(-nt/\tau_s) \tag{58}$$

This is an input parameter in the calculation of the nonlinear relaxation modulus $G(t, \gamma)$.

C. Effect of Small Polydispersity. Polydispersity has strong effect both on arm and cross-bar relaxation time. We (approximately) correct for the effect of polydispersity in relaxation spectrum by replacing monodisperse relations times i.e., τ_a and τ_b by their estimated mean times, respectively, for the polydisperse system.

C.1. Polydispersity in Arm Retraction Time. In this section, we derive the relationship between mean and variance of (total) arm retaction time and polydispersity in arm molecular mass. Even weak polydispersity may have a very strong effect on the component relaxation times in branched polymer melts because of the exponential "amplification factors" from dangling arms. The polydispersity in arm length is $M_{wa}/M_{na} = 1 + \epsilon_a$, where M_{wa} and M_{na} are weight- and number-averaged arm molecular mass, respectively. The complete arm retraction time is exponentially related to arm molecular mass M_a (i.e., $\tau_a = \tau_a(1) = \tau_{0_a}\exp(\nu' M_a/M_e)$). The relaxation time τ is a function of random arm weight (length), M_a, and τ_{0_a} is assumed to have weak dependence on molecular weight. If the density distribution function for the molecular mass is $W(M_a)$, the density distribution function for the relaxation time is given as

$$W(\tau_a) = \frac{W(M_a = (M_e/\nu')\ln(\tau_a/\tau_{0_a}))}{|d\tau(M_a(M_e/\nu')n(\tau_a/\tau_{0_a}))/dM_a|} \tag{59}$$

where $|d\tau(M_a = (M_e/\nu')\ln(\tau_a/\tau_{0_a}))/dMa| = \nu'/M_e$.

The nth moment of $Y = (M_e/\nu')\ln(\tau_a/\tau_{0_a})$ is defined as

$$\begin{aligned}\langle Y^n\rangle_\tau &= \int d\tau\,((M_e/\nu')\ln(\tau_a/\tau_{0_a}))^n\, W(\tau)\\ &= \int d\tau((M_e/\nu') \times \\ &\qquad \ln(\tau_a/\tau_{0_a}))^n \frac{W(M_a = (M_e/\nu')\ln(\tau_a/\tau_{0_a}))}{|d\tau(M_a = (M_e/\nu')\ln(\tau_a/\tau_{0_a}))/dM_a|}\\ &= \int dM_a M_a^n W(M_a)\\ &= \langle M_a^n\rangle_M\end{aligned} \tag{60}$$

where $\langle\cdot\rangle_M$ and $\langle\cdot\rangle_\tau$ are averages taken over molecular arm mass and molecular arm retraction time, respectively.

The important conclusion from eq 60 is that the nth moment of logarithmic relaxation time is equal to the nth moment of arm molecular mass.

$$\langle Y^n\rangle_\tau = \langle M_a^n\rangle_M \tag{61}$$

The average arm molecular mass is related to the first moment of logarithmic relaxation time as

$$\langle M_a\rangle_M = \langle Y\rangle_\tau = \langle (M_e/\nu')\ln(\tau/\tau_0)\rangle_\tau \tag{62}$$

The definition of polydispersity in arm molecular weight is

$$\frac{M_{wa}}{M_{na}} = \frac{\langle M_a^2\rangle_M}{\langle M_a\rangle_M^2} = \frac{\langle Y^2\rangle_\tau}{\langle Y\rangle_\tau^2} \tag{63}$$

The relaxation time τ_a in eqs 62 and 63 is replaced by the sum of mean and fluctuating parts, i.e., $\tau_a = \langle\tau_a\rangle + \tilde{\tau}$, and expanding these equations up to second order in $\tilde{\tau}/\langle\tau_a\rangle$, we obtain

$$(M_e/\nu')\,[\ln(\langle\tau_a\rangle/\tau_{0_a}) - \langle\tilde{\tau}^2\rangle/2\langle\tau_a\rangle^2] \approx \langle M_a\rangle_M = M_n \tag{64}$$

and

$$\langle\tilde{\tau}^2\rangle/\langle\tau_a\rangle^2 \approx \epsilon_a \ln^2(\langle\tau_a\rangle/\tau_{0_a}) \tag{65}$$

Combining eqs 64 and 65 and substituting $Z_a = \ln(\langle\tau_a\rangle/\tau_{0_a})$ and $s_{na} = M_{na}/M_e$, we obtain

$$Z_a^2 - \frac{2}{\epsilon_a}Z_a + \frac{2\nu' s_{na}}{\epsilon_a} = 0 \tag{66}$$

The physically correct solution of eq 66 is

$$Z_a = \frac{1}{\epsilon_a}\,[1 - (1 - 2\nu' s_{na}\epsilon)^{1/2}]$$

$$= \nu' s_{na} + \frac{(\nu' s_{na})^2}{2}\epsilon_a + \frac{(\nu' s_{na})^3}{2}\epsilon_a^2 + \ldots \tag{67}$$

The mean (total) arm retraction time is

$$\langle\tau_a\rangle = \tau_{0_a}\exp(Z) \approx \tau_{0_a}\exp\left(\nu' s_{na} + \frac{(\nu' s_{na})^2}{2}\epsilon_a + \frac{(\nu' s_{na})^3}{2}\epsilon_a^2\right)$$

The variance in (total) arm retraction time is

$$\langle\tilde{\tau}_a\rangle = \epsilon Z_a^2\,\tau_{0_a}^2\exp(2Z_a)$$

This analysis suggests that the polydispersity correction in arm relaxation time is obtained by replacing s_a by s_{ar}, i.e., renormalized value of arm entanglement lengths where s_{ar} is

$$s_{ar} = Z_a/\nu' \approx s_{na} + \frac{\nu' s_{na}^2}{2}\epsilon_a + \frac{\nu'^2 s_{na}^3}{2}\epsilon_a^2$$

$$\langle\tau_a(x_a)\rangle = \tau_a(x_a, s_a \rightarrow s_{ar}) \tag{68}$$

C.2. Polydispersity in Backbone Relaxation Time. Here we derive the relationship between the mean and variance of backbone retaction time and polydispersity in backbone molecular mass. The polydispersity in backbone length is $M_{wb}/M_{nb} = 1 + \epsilon_b$, where M_{wb} and M_{nb} are weight-averaged and number-averaged backbone molecular mass, respectively. The backbone retraction time for $x_b = x_c$ is exponentially related to backbone molecular mass M_b (i.e., $\tau_b = \tau_b(x_b = x_c) = \tau_{0_b}\exp(\nu_b M_b/M_e)$ where τ_{0_b} is a weak function of M_b and $\nu_b = 15\phi_b^\alpha(1 - (1 - x_c)^{\alpha+1}(1 + (1 + \alpha)x_c))/8(1 + \alpha)(2 + \alpha)$. The relaxation time τ_b is a function of random backbone molecular weight (length), M_b, and τ_{0_b} is assumed to have weak dependence on molecular weight.

The mean and variance backbone retraction time is obtained by a method similar to that we discussed above for arm dynamics. The mean backbone retraction time is

$$\langle\tau_b\rangle \approx \tau_{0_b}\exp\left(\nu_b s_{nb} + \frac{(\nu_b s_{nb})^2}{2}\epsilon_b + \frac{(\nu_b s_{nb})^3}{2}\epsilon_b^2\right)$$

where s_b is the number-average backbone entanglement length. The variance in backbone retraction time is

$$\langle\tilde{\tau}_b^{\,2}\rangle \approx \epsilon_b Z_b^2\,\tau_{0_b}^2\exp(2Z_b)$$

$$Z_b \approx \nu_b s_{nb} + \frac{(\nu_b s_{nb})^2}{2}\epsilon_b + \frac{(\nu_b s_{nb})^3}{2}\epsilon_b^2 \tag{69}$$

This analysis suggests that the polydispersity correction in backbone relaxation time is obtained by replacing s_b by s_{br}, i.e., a renormalized value of backbone entanglement lengths where s_{br} is

$$s_{br} \approx s_{nb} + \frac{\nu_b s_{nb}^2}{2}\epsilon_b + \frac{\nu_b^2 s_{nb}^3}{2}\epsilon_b^2$$

$$\langle\tau_b(x_b)\rangle \approx \tau_b(x_b, s_b \rightarrow s_{br}) \tag{70}$$

It is important to note that we have not assumed any specific statistics for deriving these results except small polydispersity. The values of ϵ_a and ϵ_b are found from rheological fits of data and are in reasonable agreement with experimental polydispersity in H-polymer samples (ϵ). The values of ϵ, ϵ_a and ϵ_b, are tabulated in Table 2.

D. Random Phase Approximation for Polymers in Tubes. The assumptions underlying the tube model used in this paper can be summarized as follows: (i) the tubes deform affinely, (ii) the tube diameter remains constant, and (iii) all chains retract by the same degree. If we wish to make quantitative comparison between the tube model and scattering experiments, then it is necessary to use these assumptions to predict the scattering pattern. Because of the success of the random phase approximation in describing scattering patterns from equilibrated copolymer melts, it is natural to seek a generalization of the RPA for the stretched melt case. We shall outline below the steps required to overcome this significant theoretical challenge. Further details may be found elsewhere.[37]

It is important first to stress the physical picture implied by the application of the tube model to the RPA in the neutron scattering experiments. The melt is stretched, and the time allowed for chain retraction before a rapid quench prevents any further polymer motion. Between the stretch and the quench, the fastest degrees of freedom associated with local chain variables have sufficient time for rearrangement and exploration of phase space. However, the slow degrees of freedom associated with the polymer tubes do not have sufficient time to relax. It is necessary to make a formal separation between the fast and slow variables. The fast variables may be treated as annealed on the experimental time scale, whereas the slow variables are effectively quenched and must be treated as such. Moreover, after a stretch, the quenched tube variables are no longer in an equilibrium configuration. Ultimately, we shall need to average over both quenched

and annealed variables (with care as to where the averages are taken). We shall denote averages over annealed variables by angular brackets, $\langle\cdots\rangle$, and averages over quenched variables by an overbar, $\overline{(\cdots)}$.

In the melt prior to stretching, the chains are free to fluctuate subject to the incompressibility constraint. This constraint leads to chain−chain correlations, and the resulting concentration fluctuations of the labeled monomers are well-described by the standard RPA. However, the chains are also confined to their tube and so the tube configurations must be consistent with the possible configurations of the incompressible melt; the tubes take on an equilibrium configuration. Just as there are correlations between chains, there are also correlations between their tubes. On stretching, the tubes deform affinely and the variables associated with them are quenched so the tube−tube correlations are preserved. This means that concentration variations on large length scales are "frozen in" by the tube constraints and cannot immediately relax.

On length scales smaller than the tube diameter, the chains are still free to fluctuate within their tubes and significant fluctuation occurs on the experimental time scale. On these length scales, there is no memory of the initial melt configuration, and no concentration variations are frozen in. However, the concentration fluctuations after the stretch are still subject to the incompressibility of the system.

From the above description, it is clear that we need to account for interactions between chains both before and after the stretch. After the stretch, the position of monomer l on chain α is $\mathbf{r}_l^\alpha$, and we define Fourier transformed densities of the labeled (A) monomers and unlabeled (B) monomers as

$$\rho_{\mathbf{q}}^{\mathrm{A}} = \sum_{\alpha,l} y_l^\alpha \exp(i\mathbf{q}\cdot\mathbf{r}_l^\alpha)$$

$$\rho_{\mathbf{q}}^{\mathrm{A}} = \sum_{\alpha,l} (1 - y_l^\alpha) \exp(i\mathbf{q}\cdot\mathbf{r}_l^\alpha) \tag{71}$$

where $y_l^\alpha = 1$ if the monomer is labeled and $y_l^\alpha = 0$ otherwise. Before the stretch, the position of monomer l on chain α is $\mathbf{x}_l^\alpha$ and we define the total monomer density

$$\varphi_{\mathbf{q}} = \sum_{\alpha,l} \exp(i\mathbf{q}\cdot\mathbf{E}\cdot\mathbf{x}_l^\alpha) \tag{72}$$

Notice that the sum in $\varphi_{\mathbf{q}}$ is over all A and B monomers. After imposition of incompressibility, $\varphi_{\mathbf{q}}$ is trivial but will be an essential tool in the procedure before taking the incompressible limit. We include the strain tensor $\mathbf{E}$ in this definition to bring the $\mathbf{x}_l^\alpha$ into the same space as the $\mathbf{r}_l^\alpha$, thus avoiding problems with translational symmetry in later averages.

The formal RPA result for the scattering function subject to incompressibility in the melt after the stretch and quenched tube variables is

$$S(\mathbf{q}) = \frac{T_{\mathbf{q}}^{\mathrm{AA}} T_{\mathbf{q}}^{\mathrm{BB}} - (T_{\mathbf{q}}^{\mathrm{AB}})^2}{(T_{\mathbf{q}}^{\mathrm{AA}} + T_{\mathbf{q}}^{\mathrm{BB}} + 2T_{\mathbf{q}}^{\mathrm{AB}})} + \frac{\Delta_{\mathbf{q}}^{\mathrm{AA}}(T_{\mathbf{q}}^{\mathrm{BB}} + T_{\mathbf{q}}^{\mathrm{AB}})^2 + \Delta_{\mathbf{q}}^{\mathrm{BB}}(T_{\mathbf{q}}^{\mathrm{AA}} + T_{\mathbf{q}}^{\mathrm{AB}})^2 - 2\Delta_{\mathbf{q}}^{\mathrm{AB}}(T_{\mathbf{q}}^{\mathrm{AA}} + T_{\mathbf{q}}^{\mathrm{AB}})(T_{\mathbf{q}}^{\mathrm{BB}} + T_{\mathbf{q}}^{\mathrm{AB}})}{(T_{\mathbf{q}}^{\mathrm{AA}} + T_{\mathbf{q}}^{\mathrm{BB}} + 2T_{\mathbf{q}}^{\mathrm{AB}})^2} \tag{73}$$

where the structure factors $T_{\mathbf{q}}$ and $\Delta_{\mathbf{q}}$ will be defined below. This expression represents a generalization of the model-dependent result first derived by Brereton and Vilgis.[39] Their result was derived for a specific model and did not allow for correlations between A and B monomers.

There are two types of structure factor which must be calculated in the above equation (73). The first is of type

$$\Delta_{\mathbf{q}}^{\mathrm{IJ}} = \overline{\langle\rho_{\mathbf{q}}^{\mathrm{I}}\rangle_0\langle\rho_{-\mathbf{q}}^{\mathrm{J}}\rangle_0} \tag{74}$$

where the labels I and J can each be either A or B. The annealed averages are calculated in the absence of chain−chain interactions (denoted by the subscript 0) but subject to quenched tube variables. The average over these quenched variables must include correlations between the tubes due to incompressibility in the melt prior to the stretch. The structure factors of type $\Delta_{\mathbf{q}}^{\mathrm{IJ}}$ are related to the nonzero mean of the concentration profile due to quenched variables.

The second type of structure factor is

$$T_{\mathbf{q}}^{\mathrm{IJ}} = \overline{\langle\rho_{\mathbf{q}}^{\mathrm{I}}\rho_{-\mathbf{q}}^{\mathrm{J}}\rangle_0 - \langle\rho_{\mathbf{q}}^{\mathrm{I}}\rangle_0\langle\rho_{-\mathbf{q}}^{\mathrm{J}}\rangle_0} \tag{75}$$

which is related to fluctuations about the mean of the frozen-in concentration fluctuations.

These two types of structure factor may be written in terms of single-chain structure factors, calculated in the absence of chain−chain interactions in the melt prior to stretch. To do this, an RPA calculation is used to relate the density fields $\rho_{\mathbf{q}}^{\mathrm{A}}$, $\rho_{\mathbf{q}}^{\mathrm{B}}$, and $\varphi_{\mathbf{q}}$ in the absence of any interactions (in this limit $\varphi_{\mathbf{q}}$ can be nonzero). Then, interactions are introduced that enforce incompressibility in the melt prior to stretching (i.e. they enforce $\varphi_{\mathbf{q}}$). There are four important types of single-chain structure factor:

$$\begin{aligned}
\Delta_{0\mathbf{q}}^{\mathrm{IJ}} &= \overline{\langle\rho_{\mathbf{q}}^{\mathrm{I}}\rangle_0\langle\rho_{-\mathbf{q}}^{\mathrm{J}}\rangle_0}^0 \\
T_{0\mathbf{q}}^{\mathrm{IJ}} &= \overline{\langle\rho_{\mathbf{q}}^{\mathrm{I}}\rho_{-\mathbf{q}}^{\mathrm{J}}\rangle_0 - \langle\rho_{\mathbf{q}}^{\mathrm{I}}\rangle_0\langle\rho_{-\mathbf{q}}^{\mathrm{J}}\rangle_0}^0 \\
D_{\mathbf{q}}^{\mathrm{I}} &= \overline{\langle\rho_{\mathbf{q}}^{\mathrm{I}}\rangle_0\langle\varphi_{-\mathbf{q}}\rangle_0}^0 \\
S_{\mathbf{q}}^{\mathrm{tot}} &= \overline{\langle\varphi_{\mathbf{q}}\varphi_{-\mathbf{q}}\rangle_0}^0
\end{aligned} \tag{76}$$

where the superscript 0 denotes the absence of tube−tube correlations in the quenched average. We find

$$\begin{aligned}
T_{\mathbf{q}}^{\mathrm{IJ}} &= T_{0\mathbf{q}}^{\mathrm{IJ}} \\
\Delta_{\mathbf{q}}^{\mathrm{IJ}} &= \Delta_{0\mathbf{q}}^{\mathrm{IJ}} - \frac{D_{\mathbf{q}}^{\mathrm{I}} D_{\mathbf{q}}^{\mathrm{J}}}{S_{\mathbf{q}}^{\mathrm{tot}}}
\end{aligned} \tag{77}$$

Together, the equations 73, 76, and 77 represent the generalization of the standard RPA result (21) to the stretched melt with quenched but correlated tube variables. It can be shown that these equations reduce to eq 21 in certain limits, most importantly in the case where no stretch takes place and the tubes are in an equilibrium configuration. As in the standard RPA case, the structure factors in eq 76 must be calculated from some convenient model for the polymer melt. We now briefly describe the model used to calculate the H-polymer scattering functions.

We take as our description of the polymer tubes a modified version of the Warner−Edwards model[40] originally used to describe chain localization in networks. In this model, the chains are localized by harmonic potentials acting on individual monomers. A stretch may be imposed by affine deformation of these harmonic potentials, corresponding to affine deformation of the tube. However, in the melt case, we must account for the additional mechanism of retraction, and this presents problems for the Warner−Edwards description of the tube because the localizing potentials do not allow movement of chains along the tube. We must impose the retraction process on the model. In the melt, the chains retract along the tube mean path $\hat{\mathbf{r}}(l)$, for which there exists a direct analogue in the Warner−Edwards model. A retraction along the tube mean path (which has deformed affinely) may be represented in the Warner−Edwards model by prescribing a transformation of $\hat{\mathbf{r}}(l)$ via

$$\hat{\mathbf{r}}(l) \rightarrow \mathbf{E}\cdot\hat{\mathbf{r}}\left(\frac{\lambda l}{\alpha(\mathbf{E})}\right) \tag{78}$$

The retraction is represented by "sliding" the monomer l to the initial position in the tube of the "$\lambda l/\alpha(\mathbf{E})$th" monomer. Note that this prescription involves something of a "pre-average" in that the retraction along the tube is deemed to be uniform and not dependent on the local tube orientation. We have not, to date, found an alternative prescription which remains workable.

The results for a melt of *linear* chains of molecular weight N are as follows. We use a normalized wavevector $Q_\mu = q_\mu b\,(N/6)^{1/2}$ (μ = principle strain directions 1, 2, and 3). We also introduce the normalized tube diameter $\zeta^2 = [(6)^{1/2}a^2]/(2Nb^2)$ and the contour length coordinates $x = l/N$ and $y = l'/N$. If $\gamma = \alpha(\mathbf{E})/\lambda$, then the bare correlation functions are of form

$$T_{0\mathbf{q}} = N\int \mathrm{d}x \int \mathrm{d}y \exp\left[-\sum_\mu Q_\mu^2 \epsilon_\mu^2 \left\{\frac{|x-y|}{\gamma} - \zeta^2\left(1-\exp\left(-\frac{|x-y|}{\gamma\zeta^2}\right)\right)\right\}\right] \times \left\{\exp\left[-\sum_\mu Q_\mu^2\zeta^2\left(1-\exp\left(-\frac{|x-y|}{\zeta^2}\right)\right)\right] - \exp[-\sum_\mu Q_\mu^2\zeta^2]\right\} \tag{79}$$

$$\Delta_{0\mathbf{q}} = N\exp[-\sum_\mu Q_\mu^2\zeta^2] \times \int \mathrm{d}x \int \mathrm{d}y \exp\left[-\sum_\mu Q_\mu^2\epsilon_\mu^2\left\{\frac{|x-y|}{\gamma} - \zeta^2\left(1-\exp\left(-\frac{|x-y|}{\gamma\zeta^2}\right)\right)\right\}\right] \tag{80}$$

$$D_{\mathbf{q}} = N\exp\left[-\sum_\mu Q_\mu^2\zeta^2\left(\frac{1+\lambda\epsilon_\mu^{\,2}}{2}\right)\right] \times \int \mathrm{d}x \int \mathrm{d}y \exp\left[-\sum_\mu Q_\mu^2\epsilon_\mu^2\left\{\left|\frac{x}{\gamma}-y\right| - \zeta^2\left(1-\exp\left(-\frac{1}{\zeta^2}\left|\frac{x}{\gamma}-y\right|\right)\right)\right\}\right] \tag{81}$$

In all of these expressions, the range of integration for the contour length coordinates (x and y) must be chosen to reflect the required correlation function. For example, in calculating $T_{0\mathbf{q}}^{\mathrm{AB}}$, the x integral should be over all A monomers and the y integral over all B monomers. In the expression for $D_{\mathbf{q}}$, the x contour variable relates to the chain after the stretch, and the y contour variable relates to the chain before the stretch. Care must be taken to ensure that the point $x = y = 0$ is taken to be at a monomer that does not change position within the tube under the retraction (in a symmetric polymer, this point is at the center).

In these expressions, we have taken the localizing potentials to be isotropic. Although it has been suggested in networks that the potentials should couple to strain,[43] we did not find any significant improvement in the quality of the fit by modifying the tube potential as suggested in these references.

The final correlation function to be calculated in eq 76 is $S_{\mathbf{q}}^{\mathrm{tot}}$. If all the chains are identical, this is simply proportional to the standard single chain structure factor $g(\mathbf{q})$ (the Debye function if the chains are linear) but is affinely deformed via $\mathbf{E}$

$$S_{\mathbf{q}}^{\mathrm{tot}} = nN^2 g(\mathbf{q}\cdot\mathbf{E}) \tag{82}$$

Correlation functions were calculated for the H-polymer case using expressions based on those above, but accounting for several complications arising from the presence of branch points:

(1) Correlations must be calculated for a chain in the same tube but retracted by different degrees at either side of a branch point (in general $\lambda_{\mathrm{crossbar}} \neq \lambda_{\mathrm{arm}}$).

(2) After branch-point withdrawal, there are sections of tube containing two chains. These chains are joined at a single end but lie within different tube arms at the other end.

(3) During the experimental time, about 0.25 of each arm relaxes by breathing modes, giving reoriented 'dangling ends'. These were dealt with in a manner analogous to that in Read.[38]

E. Table of Parameter Values. Table 4 gives the values of physical parameters of moduli and time scales used in the linear (at 25 °C) and nonlinear (at 90 °C in brackets) rheological experiments. The variation in plateau moduli values has a range of causes, from partial filling of rheometer gap to slight changes in density. The time scale shifts between the two temperatures used are entirely consistent with WLF parameters for polyisoprene.

Table 4. Physical Parameters

polymer	τ_{rep}(s)	τ_{a}(s)	G_{o} (Pa) × 10^{-5}	τ_{s}(s) at 90 °C
H110B20A	300 (8.35)	0.41 (0.013)	5.5	1.14
H160B40A	21 000	112	7.0	
H110B52A	18 400	203	5.3	
H200B65A	6.24×10^6	16 445	4.6	

References and Notes

(1) Quack, G.; Hadjichristidis, N.; Fetters, L. J.; Young, R. N. *Ind. Eng. Chem. Prod. Res. Dev.* **1980**, *19*, 587.

(2) Doi, M.; Edwards, S. F. *The Theory of Polymer Dyamics*; Clarendon: Oxford, 1986.

(3) Osaki, K.; Kurata, M. *Macromolecules* **1980**, *13*, 671.

(4) Rubinstein, M. *Phys. Rev. Lett.* **1987**, *59*, 1946. Deutsch, J. M.; Madden, T. L. *J. Chem. Phys.* **1989**, *91*, 3252. O'Connor, N. P. T.; Ball, R. C. *Macromolecules* **1992**, *25*, 5677.

(5) Doi, M.; Kuzuu, N. Y. *J. Polym. Sci., Polym. Lett. Ed.* **1980**, *18*, 775. Pearson, D. S.; Helfand, E. *Macromolecules* **1984**, *19*, 888. Ball, R. C.; McLeish, T. C. B. *Macromolecules* **1989**, *22*, 1911.

(6) For recent reviews, see: Rubinstein, M.; McLeish, T. C. B. In *Theoretical Challenges in the Dynamics of Complex Fluids*; McLeish, T. C. B., Ed.; Kluwer: Dordrecht, The Netherlands, 1997. McLeish, T. C. B.; Milner, S. T. *Adv. Polym. Sci.* **1999**, *143*, 195.
(7) Fetters, L. J.; Kiss, A. D.; Pearson, D. S.; Quack, G. F.; Vitus, F. J. *Macromolecules* **1993**, *26*, 647.
(8) Milner, S. T.; McLeish, T. C. B. *Macromolecules* **1997**, *30*, 2159.
(9) Adam, M.; Delsanti, M. *J. Phys. (Paris)* **1984**, *45*, 1513.
(10) Colby, R. H.; Rubinstein, M. *Macromolecules* **1990**, *23*, 2753.
(11) Fetters, L. J.; Lohse, D. J.; Richter, D.; Witten, T. A.; Zirkel, A. *Macromolecules* **1994**, *27*, 4639.
(12) Milner, S. T.; McLeish, T. C. B. *Phys. Rev. Lett.* **1998**, *81*, 725.
(13) Blottière, B.; McLeish, T. C. B.; Hakiki, A.; Young, R. N.; Milner, S. T. *Macromolecules* **1998** *31*, 9295.
(14) Milner, S. T.; McLeish, T. C. B.; Johnson, J.; Hakiki, A.; Young, R. N. *Macromolecules* **1998**, *31*, 9345.
(15) Meissner, J. *Pure Appl. Chem.* **1975**, *42*, 551.
(16) Osaki, K. *Rheol. Acta* **1993**, *32*, 429.
(17) Roovers, J. *Macromolecules* **1984**, *17*, 1196.
(18) McLeish, T. C. B. *Macromolecules* **1988**, *21*, 3639.
(19) Roovers, J.; Graessley, W. W. *Macromolecules* **1981**, *14*, 766.
(20) Yurasova, T. A.; McLeish, T. C. B.; Semenov, A. N. *Macromolecules* **1994**, *27*, 7205.
(21) McLeish, T. C. B.; Larson, R. G. *J. Rheol.* **1998**, *42*, 81.
(22) Bick, D. K.; McLeish, T. C. B. *Phys. Rev. Lett.* **1996**, *76*, 2587.
(23) Hakiki A.; Young, R. N.; McLeish, T. C. B. *Macromolecules* **1996**, *29*, 3639.
(24) Archer, L. A.; Varshney, S. K., *Macromolecules* **1998**, *31*, 6348.
(25) McLeish, T. C. B. *Phys. World* **1995**, *8*, 32.
(26) McLeish, T. C. B. In *Theoretical Challenges in the Dynamics of Complex Fluids*; McLeish, T. C. B., Ed.; Kluwer: Dordrecht, The Netherlands, 1997.
(27) McLeish, T. C. B. *Polym. Commun.* **1989**, *30*, 4.
(28) Muller, R.; Pesce, J. J.; Picot, C. *Macromolecules* **1993**, *26*, 4356.
(29) Boué, F.; Osaki, K.; Ball, R. C. *J. Polym. Sci., Part B: Polym. Phys.* **1985**, *23*, 833.
(30) Rubinstein, M.; Zurek, S.; McLeish, T. C. B.; Ball, R. C. *J. Phys. (Paris)* **1990**, *51*, 757.
(31) Ball, R. C.; McLeish, T. C. B. *Macromolecules* **1990**, *22*, 1911.
(32) Edwards, S. F. *Proc. Phys. Soc., London* **1966**, *88*, 265.
(33) Lee, C. S.; Tripp, B. C.; Magda, J. J. *Rheol. Acta* **1992**, *31*, 306.
(34) Heenan, R. K.; Penfold, J.; King, S. M. *J. Appl. Crystallogr.* **1997**, *30*, 1140.
(35) Milner, S. T.; McLeish, T. C. B. *Macromolecules* **1998**, *31*, 7479.
(36) Read, D. J. *Macromolecules* **1998**, *31*, 899.
(37) Read, D. J. *Euro. J. Phys.* **1999**, accepted for publication.
(38) Read, D. J.; McLeish, T. C. B. *Macromolecules* **1997**, *30*, 637. Read, D. J.; McLeish, T. C. B. *Phys. Rev. Lett.* **1997**, *79*, 87.
(39) Brereton, M. G.; Vilgis, T. *J. Phys. (Paris)* **1992**, 581.
(40) Warner, M.; Edwards, S. F. *J. Phys. A* **1978**, *11*, 1649.
(41) McKinley, G.; Hassager, O. *J. Rheol.* **1999**, submitted for publication.
(42) Inkson, N. I.; Harlen, O. G.; Groves, D. J.; McLeish, T. C. B. *J. Rheol.* **1999**, *43*.
(43) Straube, E.; Urban, V.; Pyckhout-Hintzen, W., Richter, D. *Macromolecules* **1994**, *27*, 7681.

MA990323J